AD-A094 870 ANALYTIC SCIENCES CORP READING MA F/G 12/1
RESEARCH IN MULTIRATE ESTIMATION AND CONTROL.(U)
DEC 80 D P GLASSON N00014-79-C-0431
UNCLASSIFIED TASC-TR-1356-1 NL

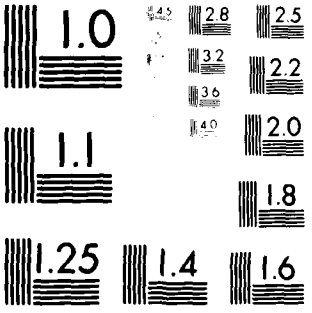

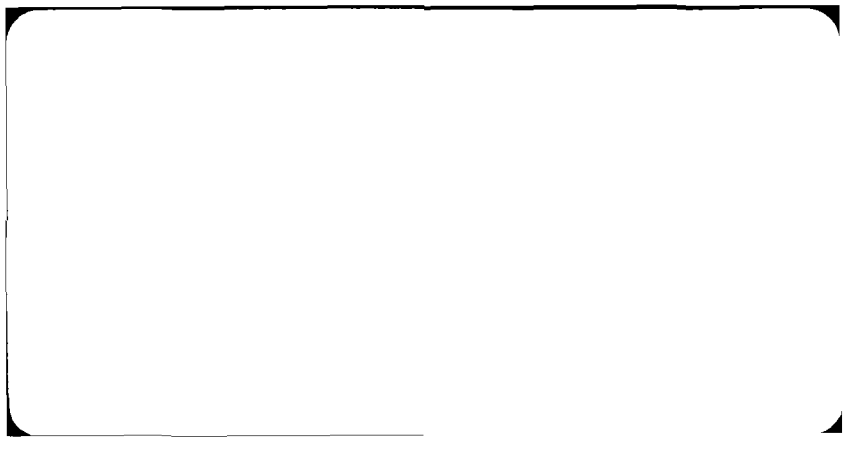

THE ANALYTIC SCIENCES CORPORATION

TR-1356-1

RESEARCH IN MULTIRATE ESTIMATION AND CONTROL

20 December 1980

Prepared for:

OFFICE OF NAVAL RESEARCH
Arlington, Virginia

Prepared by:

Douglas P. Glasson

Approved by:

Charles F. Price
E. Wayne Vinje

THE ANALYTIC SCIENCES CORPORATION
Six Jacob Way
Reading, Massachusetts 01867

UNCLASSIFIED

SECURITY CLASSIFICATION OF THIS PAGE (When Data Entered)

REPORT DOCUMENTATION PAGE	READ INSTRUCTIONS BEFORE COMPLETING FORM
1. REPORT NUMBER: TR-1356-1	2. GOVT ACCESSION NO.: AD-A094 070
3. RECIPIENT'S CATALOG NUMBER:	
4. TITLE (and Subtitle): Research in Multirate Estimation and Control	5. TYPE OF REPORT & PERIOD COVERED: Yearly Report 5/1/79 - 5/1/80
6. PERFORMING ORG. REPORT NUMBER: TR-1356-1	
7. AUTHOR(s): Douglas P. Glasson	8. CONTRACT OR GRANT NUMBER(s): N00014-79-C-0431
9. PERFORMING ORGANIZATION NAME AND ADDRESS: The Analytic Sciences Corporation, Six Jacob Way, Reading, Massachusetts 01867	10. PROGRAM ELEMENT, PROJECT, TASK AREA & WORK UNIT NUMBERS
11. CONTROLLING OFFICE NAME AND ADDRESS: Office of Naval Research, Arlington, Virginia	12. REPORT DATE: December 1980
	13. NUMBER OF PAGES: 122
14. MONITORING AGENCY NAME & ADDRESS (if different from Controlling Office)	15. SECURITY CLASS. (of this report): Unclassified
	15a. DECLASSIFICATION/DOWNGRADING SCHEDULE

16. DISTRIBUTION STATEMENT (of this Report)

Approved for public release; distribution unlimited.

17. DISTRIBUTION STATEMENT (of the abstract entered in Block 20, if different from Report)

18. SUPPLEMENTARY NOTES

19. KEY WORDS (Continue on reverse side if necessary and identify by block number)

Digital Control Systems
Flight Control Systems
Kalman Filters
Multiple Sample Rate Control
Optimal Control
Optimal Estimation

20. ABSTRACT (Continue on reverse side if necessary and identify by block number)

A new approach to multirate control system synthesis based on optimal estimation and control theory is developed. The new techniques obviate dimensionality problems typical of classically-based design techniques and offer a systematic procedure for designing to desired closed-loop specifications. Mathematical derivations of the optimal multirate state estimator, regulator, and proportional-plus-integral controllers are presented. The

DD FORM 1 JAN 73 1473 EDITION OF 1 NOV 65 IS OBSOLETE

UNCLASSIFIED

SECURITY CLASSIFICATION OF THIS PAGE (When Data Entered)

20. Abstract (Continued)

transient response and robustness properties of multirate systems designed by the present techniques are investigated through examples.

PREFACE

This investigation was conducted by The Analytic Sciences Corporation, Reading, Massachusetts, from 1 May 1979 through 1 May 1980, under Contract N00014-79-0431 for the Office of Naval Research, Washington, D.C. It was sponsored by the Vehicle Technology Program headed by Mr. David Siegel. Mr. Robert Von Husen served as the Navy Scientific Officer for the program. Approval for public release of this report was granted by Dr. Stuart Brodsky of the Mathematics Program.

Mr. Douglas P. Glasson was the principal investigator in this study. The technical contributions to this project of Mr. John R. Broussard are acknowledged.

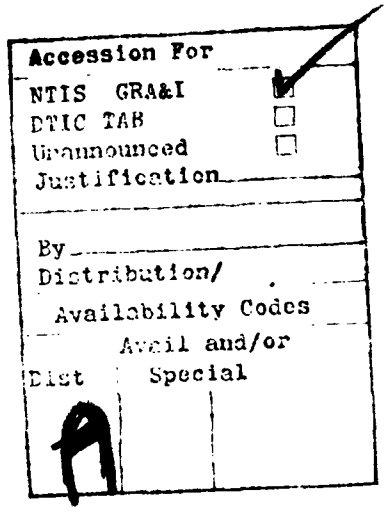

TABLE OF CONTENTS

TABLE OF CONTENTS (Continued)

LIST OF FIGURES

LIST OF FIGURES (Continued)

LIST OF TABLES

1. INTRODUCTION

1.1 BACKGROUND

The practical need for multiple sample rate flight control systems is a basic consequence of the finite computing capabilities of onboard digital computers. Although digital computer technology continues to advance significantly, new and expanded software requirements for such functions as navigation, display, and control manage to keep pace with improvements in computational capability. Accordingly, the flight control system designer is always allocated a fixed (and usually limiting) amount of computational capability to implement a control design. In modern flight control system applications, the problem of implementing a desired algorithm within a limited computational capability is compounded by a need to accommodate high frequency bending mode effects. Functions associated with bending effects (i.e., instrument output filtering or active structural control) typically demand sample rates an order of magnitude higher than is necessary for suitable control of rigid body modes of vehicle motion. Faced with widely varying sample rate requirements among the dynamic modes of the vehicle, a multirate control structure is the solution to computational limitations.

Synthesizing a multirate control system to meet desired specifications has been a difficult task. Ad hoc approaches have typically been used, in which a suitable analog design is converted to a digital design via Tustin transform techniques. In this case multirate designs are generated by a trial-and-error process of running the low bandwidth compensating elements

at low sample rates and evaluating the resulting system performance via simulation. Classically based techniques for multirate system analysis (e.g., Sklansky's identity) are available (Refs. 2, 3, and 4); however, these techniques suffer staggering growth of dimensionality in application and are typically usable for only very low order systems. Such techniques are also analysis, as opposed to synthesis, approaches; hence, creating a control design is still an iterative procedure. In the present report, multirate design techniques based on optimal control are developed which obviate dimensionality problems characteristic of classical techniques. In addition, these techniques offer a systematic method for converting a desired analog control design to an equivalent multirate digital design without approximation.

The multirate control design procedure described in the present report builds upon some recent results in optimal filtering for the case of periodic observations (Ref. 1). Mathematically, it has been shown that if the plant matrices, noise covariances, and measurements of a Kalman filter formulation are periodically time-varying, then the filter error covariance matrix and, hence, the filter gains are periodically time-varying in steady-state. In this report, the control synthesis problem is considered for the case of periodic control computations. In a manner analogous to the filtering problem, the steady-state optimal regulator solution is periodic with a period equal to the number of control computation cycles over which the control update sequence repeats itself. This property of the multirate optimal regulator is illustrated in the report through examples.

1.2 SUMMARY OF RESULTS

The major results obtained in this investigation are:

- Basic formulation of the optimal multirate estimator/regulator design problems.
- Design-to-specification procedure for multirate control systems.
- Extension of the multirate control design formulation to proportional-plus-integral control structures.
- A methodology to evaluate the relative stability (robustness) of multirate control systems.
- A preliminary investigation of performance/computation optimization for multirate control systems.

All of the accomplishments listed are illustrated through design examples.

The basic formulation of the optimal multirate estimator/regulator design problem is simply a matter of accounting for periodic time-variations of measurements and controls. The optimal linear filter and regulator formulations accommodate these time-variations; the conditions for periodic steady-state solutions of these design problems are established in Ref. 1.

A three-step procedure for designing a multirate digital controller to specifications is prescribed. This procedure entails: designing a continuous-time optimal control which meets desired specifications; using the state and control weighting matrices for the continuous-time controller to derive weighting matrices for the equivalent single-rate digital controller by the methods of Ref. 5; and deriving multirate state and control

weighting matrices from the single-rate matrices. The continuous-time, single-rate digital, and multirate digital systems designed from the three sets of weighting matrices optimize the same cost functional (Ref. 5); the two digital systems optimize the cost functional under the constraint of piecewise linear controls. In addition, the multirate weighting matrices can be derived from partitions of the single-rate matrices; hence, existing software packages for designing single-rate controllers can be utilized in multirate designs.

Extension of the multirate control design methodology to proportional-plus-integral (PI) structures is straightforward. The mathematical formulation of the PI design problem involves augmentation of the plant dynamics with control integration states; again the three-step design procedure can be followed to achieve desired system specifications.

A covariance analysis procedure is developed to investigate the robustness of multirate control systems. Although the design-to-specification procedure produces systems having equivalent transient responses, the ability of a multirate system to reject disturbances varies with the sample rate and control sequence. For example, if continuous-time, single-rate, and multirate (with one or more controls computed at a lower rate) regulators are designed by the three step procedure all three will have the same transient response characteristics; however, the disturbance rejection properties of the single-rate system will be degraded from those of the continuous-time system and, similarly, the multirate systems disturbance rejection properties are degraded from those of the single rate system. A design example is presented that illustrates robustness trends as a function of control computation schedule.

Finally, a preliminary investigation of performance/computation tradeoffs is presented. This investigation suggests development of a mathematical optimization procedure for determining sample rates and control schedules of multirate systems.

1.3 ORGANIZATION OF THE REPORT

This report addresses the formulation and solution of the optimal estimator/regulator design problems, design of multirate proportional-plus-integral controllers, and evaluation of robustness of multirate controllers. The basic optimal multirate estimation and control formulations are covered in Chapter 1; design examples are also discussed in Chapter 1. Extensions of the multirate control design procedure to proportional-plus-integral structures are presented in Chapter 2; again a design example illustrates the results of the design procedure. Robustness of multirate controllers is investigated through an example in Chapter 3. Conclusions and recommendations are presented in Chapter 4.

2 OPTIMAL MULTIRATE ESTIMATION AND CONTROL

2.1 OVERVIEW

The purpose of this chapter is to develop the basic multirate estimator and regulator structures. Systematic synthesis techniques for these structures are outlined and, through an example, typical properties of the structures are described.

The multirate synthesis technique developed utilizes two important properties of the optimal estimator/regulator formulations:

- The optimal linear filter and regulator formulations accommodate time-varying measurement policies and control computation rates.
- The optimal filter and regulator solutions reach periodic steady-states for periodic sampling and control computation rates.

The first property is one that is often overlooked; i.e., the modern estimation/control synthesis techniques are typically applied to time-invariant plants or frozen-point designs of a time-varying plant. One notable exception is active multidither estimation in adaptive optics (Ref. 6); the introduction of dither causes the measurement matrix of the extended Kalman filter to be time-varying. The second property is a significant one, in that it leads to an extended interpretation of

steady-state filter and controller designs. Whereas the time-invariant or frozen-point applications lead to constant filter and regulator gain matrices (or quasi-static gain schedules), the periodically time-varying case leads to sets of filter and regulator gain matrices which are repeated periodically. For example, it might be desired to design an aircraft lateral controller that computes rudder commands at a significantly lower rate than aileron commands. If the aircraft lateral dynamics are represented as time-invariant, the multirate control computation policy leads to a set of control gains for rudder commands that are used at the slow rate plus a set of aileron gains that vary at the faster aileron sample rate between rudder updates. These periodic gain sets are the natural end-product of the synthesis technique described in this chapter.

In Section 2.2 multirate estimator design is outlined. The formulation of the optimal multirate regulator is developed in Section 2.3; a systematic methodology for deriving the multirate state and control error weighting matrices from specified continuous-time matrices is also described in Section 2.3. Eigenvalue-eigenvector analysis of multirate systems is covered in Section 2.4. The principles of multirate estimation and control are applied to a design example which is discussed in Section 2.5. The chapter is summarized in Section 2.6.

2.2 MULTIRATE ESTIMATOR DESIGN

It is desired to estimate the states of the linear-time-invariant stochastic process described by:

$$\underline{x}_{k+1} = \Phi \underline{x}_k + \underline{w}_k \; ; \quad \underline{w}_k \sim N(0,Q) \tag{2.2-1}$$

$$t_{k+1} - t_k = T_s \tag{2.2-2}$$

The measurements used to estimate the states are given by:

$$\underline{z}_{1_k} = H_{1_k}\underline{x}_k + \underline{v}_{1_k} \; ; \; \underline{v}_{1_k} \sim N(0,R_1) \qquad (2.2\text{-}3)$$

$$\underline{z}_{2_k} = H_{2_k}\underline{x}_k + \underline{v}_{2_k} \; ; \; \underline{v}_{2_k} \sim N(0,R_2) \qquad (2.2\text{-}4)$$

The case of the measurement $\underline{z}_{2_k}$ being available (or utilized) at a lower sample rate than $\underline{z}_{1_k}$ is of interest here; formally, this is a conventional Kalman filtering problem handled by setting H_{2_k} equal to zero at times when $\underline{z}_2$ is unavailable.

The structure of a multirate Kalman filter for the case of two sample rates is shown in Fig. 2.2-1. Here the measurement $\underline{z}_{1_k}$ is available at the "fast rate", T_s^{-1} samples per second; the measurement $\underline{z}_{2_{i\ell}}$ is available (or is utilized) only on cycles where:

$$k = i\ell \qquad (2.2\text{-}5)$$

with

$$i = 0, 1, 2, \ldots \qquad (2.2\text{-}6)$$

and

ℓ = integer period of the slow measurements (i.e., the number of fast rate periods between measurements, $\underline{z}_{2_k}$)

Accordingly, the signal paths and innovations ($\underline{v}_1$ and $\underline{v}_2$) computations indicated by the dashed lines apply only to cycles where $k = i\ell$;
i.e.:

On cycles where k = iℓ (major update):

$$\underline{z}_k^T = (\underline{z}_{1_{i\ell}}^T \mid \underline{z}_{2_{i\ell}}^T) \tag{2.2-7}$$

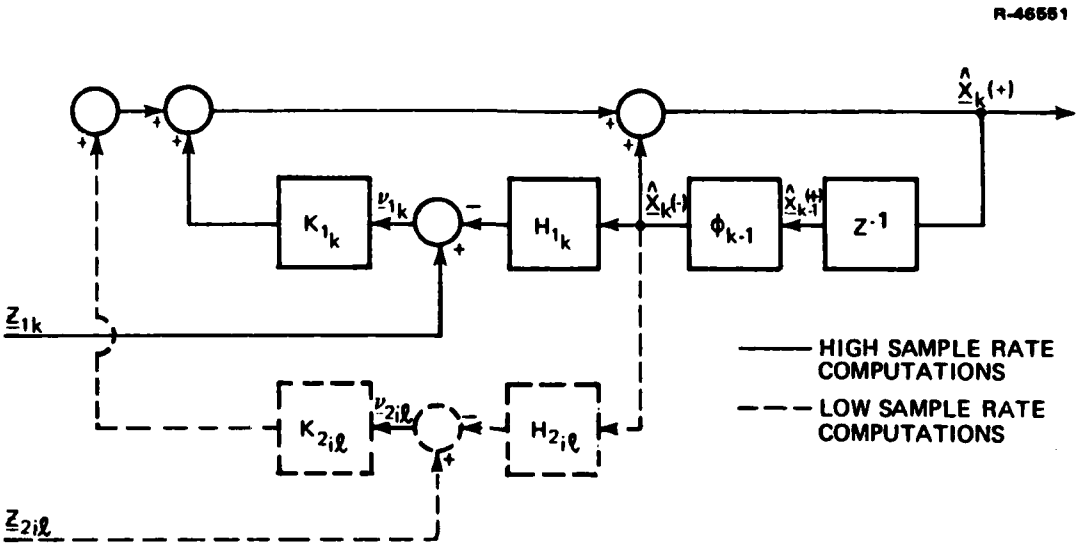

Figure 2.2-1 Multirate Kalman Filter Structure

$$H_k = \begin{bmatrix} H_{1_{i\ell}} \\ \hline H_{2_{i\ell}} \end{bmatrix} \tag{2.2-8}$$

$$\underline{v}_k^T = (\underline{v}_{1_{i\ell}}^T \mid \underline{v}_{2_{i\ell}}^T) \tag{2.2-9}$$

On cycles where k ≠ iℓ (subinterval):

$$\underline{z}_k = \underline{z}_{1_k} \tag{2.2-10}$$

$$H_k = H_{1_k} \tag{2.2-11}$$

$$\underline{\upsilon}_k = \underline{\upsilon}_{1_k} \tag{2.2-12}$$

Note that the dimensions of the measurement, measurement sensitivity, and residual matrices vary periodically; similarly, the dimension of the measurement noise covariance matrix is periodic:

$$R_k = \left[\begin{array}{c|c} R_{1_{i\ell}} & 0 \\ \hline 0 & R_{2_{i\ell}} \end{array}\right] \quad ; \quad k = i\ell \tag{2.2-13}$$

$$R_k = R_{1_k} \quad ; \quad k \neq i\ell \tag{2.2-14}$$

In Eq. 2.2-13 it is assumed that the measurement noises of the fast and slow measurements are uncorrelated.

The filter gains, K_1 and K_2 are periodic and can be derived by propagating the discrete Kalman filter covariance equation to (periodic) steady-state; i.e.,:

$$P_k(-) = \Phi P_{k-1}(+)\Phi^T + Q \tag{2.2-15}$$

$$K_k = H_k^T P_k(-)\,(H_k P_k(-) H_k^T + R_k)^{-1} \tag{2.2-16}$$

$$P_k(+) = (I - K_k H_k) P_k(-) \tag{2.2-17}$$

using the expressions for H_k and R_k given by Eqs. 2.2-8, 2.2-11, 2.2-13, and 2.2-14, respectively. The periodic steady-state gains derived by propagation of Eqs. 2.2-15 to 2.2-17 are:

$$K_k = \left[K_{1_{i\ell}} \,\vdots\, K_{2_{i\ell}} \right] \quad ; \; k = i\ell \tag{2.2-18}$$

$$K_k = K_{1_k} \quad ; \quad k \neq i\ell \tag{2.2-19}$$

As will be shown later in an example, the gains associated with the fast rate measurements, K_{1_k}, vary from sample to sample between major updates.

A heuristic interpretation of the filter structure shown in Fig. 2.2-1 is possible. Suppose, for example, that it is desired to estimate the angular rate and position of a rigid vehicle from rate gyro and inertial navigation system (INS) measurements. Assume that the rate gyro measurements are available at a high sample rate but that INS measurements (which explicitly measure angular position) are available at a much slower rate. On cycles when the INS measurements are not available, the filter estimates angular position by essentially integrating the angular rate estimates; although this provides the optimal estimate of the angular position given the available measurements, the error covariance of the angular position estimate grows with time. On cycles when the INS measurement is available, the position estimate and, hence, the estimation error covariance are "reset"; i.e., an accurate position estimate is generated by the INS measurement. This reset position estimate is then extrapolated on subsequent cycles via rate estimate integration until a new INS measurement is again available. Hence, the multirate structure is analogous to the classical concept of inner and outer loops;

the inner loop runs at a fast sample rate estimating "fast" dynamic modes and extrapolating slow modes, while the outer loop runs at a slower rate resetting extrapolation errors accumulated in the inner loop. An illustrative example of this filtering structure is given in Section 2.5.

2.3 MULTIRATE REGULATOR

2.3.1 Regulator Structure

It is assumed that a plant to controlled has continuous time dynamics given by:

$$\dot{\underline{x}}(t) = F\underline{x}(t) + G\underline{u}(t) \qquad (2.3\text{-}1)$$

where $\underline{x}$ is its state vector and $\underline{u}$ is its control vector. The control $\underline{u}$ is to be sampled and held at time instants t_k, with all elements of $\underline{u}$ possibly sampled at different rates.

The structure of a multirate optimal regulator for the case of two sample rates is shown in Fig. 2.3-1. As the block diagram indicates, one control channel, $\underline{u}_f$, is updated at a fast rate, T_s^{-1} samples per second; $\underline{u}_s$ is computed at a slower rate, $(\ell T_s)^{-1}$ samples per second, and is held between computations by a holding circuit. Recomputation of $\underline{u}_s$ is accomplished by adding an increment, $\underline{v}_k$, to the holding circuit on cycles when $k = i\ell$; on all other cycles $\underline{v}_k$ is set to zero.

The discrete time dynamics of the continuous plant are described by:

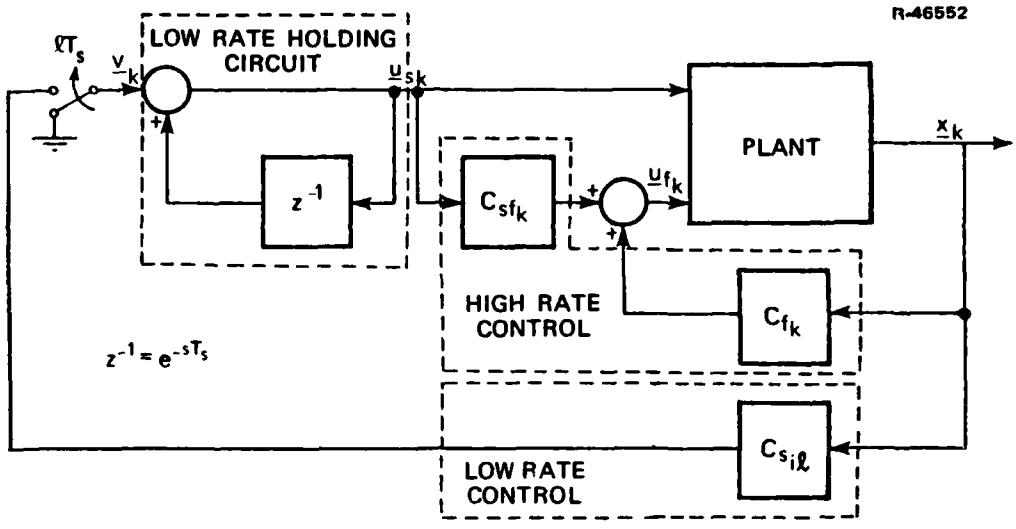

Figure 2.3-1 Multirate Regulator Structure

$$\underline{x}_{k+1} = \Phi \underline{x}_k + \Gamma_f \underline{u}_{f_k} + \Gamma_s \underline{u}_{s_k} \qquad (2.3\text{-}2)$$

where

$$\Phi = e^{FT_s}$$

$$\Gamma = \int_0^{T_s} e^{F\tau} G \, d\tau$$

Development of the multirate regulator structure requires augmentation of the natural plant dynamics with holding circuit states (i.e., to hold the slow controls between updates); the discrete time dynamics of this augmented system are given by:

$$\begin{bmatrix} \underline{x}_{k+1} \\ \hline \underline{u}_{s_{k+1}} \end{bmatrix} = \begin{bmatrix} \Phi & \Gamma_s \\ \hline 0 & I \end{bmatrix} \begin{bmatrix} \underline{x}_k \\ \hline \underline{u}_{s_k} \end{bmatrix} + \begin{bmatrix} \Gamma_f & \Gamma_s \delta_{k,i\ell} \\ \hline 0 & I \; \delta_{k,i\ell} \end{bmatrix} \begin{bmatrix} \underline{u}_{f_k} \\ \hline \underline{v}_k \end{bmatrix} \qquad (2.3\text{-}3)$$

where $\delta_{k,i\ell}$ is the Kronecker delta function.

The periodic gains -- C_{f_k}, $C_{s_{i\ell}}$, and C_{sf_k} -- are obtained by propagating the optimal regulator Ricatti equation from infinity backwards to (periodic) steady state. The derived periodic regulator gains are:

$$C_k = \left[\begin{array}{c:c} C_{f_{i\ell}} & C_{sf_{i\ell}} \\ \hdashline & C_{s_{i\ell}} \end{array}\right] \quad ; \quad k = i\ell$$

$$C_k = \left[C_{f_k} \,\vdots\, C_{sf_k}\right] \; ; \; k \neq i\ell \qquad (2.3\text{-}4)$$

Note that the dimensions of C_k change according to the number of controls that are computed on cycle k. The periodic weighting matrices, $\hat{Q}_k$, $\hat{M}_k$ and $\hat{R}_k$, used in the propagation of the Ricatti equation are derived from continuous-time control specifications; the derivation of these matrices is discussed in Section 2.3.2.

A heuristic interpretation of the multirate regulator can be made, similar to that of the multirate filter. The fast sample rate controls regulate the high frequency plant dynamics, while the slow controls regulate the slower, less dominant dynamic modes. Again, the multirate structure is analogous to the inner-loop/outer-loop structures commonly used in classical control.

One additional element of the multirate regulator structure should be noted; a crossfeed exists from the slow control channel to the fast control channel. On cycles when the outer control loop is inactive, $\underline{u}_s$ appears to be a disturbance to the plant and is "compensated" via feedforward control (computed from C_{sf_k}) to the $\underline{u}_f$ channel. The inner control

loop is "aware" that the slow controls are coarse (i.e., computed at a slower rate) and uses the C_{sf} crossfeed to accommodate this coarseness.

Extension of the two-sample-rate control structure described here to the multirate case (i.e., more than two sample rates) is straightforward. Consider organizing the plant inputs into two groups: those computed at the fastest rate, $\underline{u}_f$, and those scheduled at lower rates, $\underline{u}_s$. Again augmenting the plant dynamics with slow control holding circuits (which now are operating at multiple rates) the discrete time dynamics of the augmented system are given by:

$$\begin{bmatrix} \underline{x}_{k+1} \\ \hline \underline{u}_{s_{k+1}} \end{bmatrix} = \left[\begin{array}{c|c} \Phi & \Gamma_s \\ \hline 0 & I \end{array}\right] \begin{bmatrix} \underline{x}_k \\ \hline \underline{u}_{s_k} \end{bmatrix} + \left[\begin{array}{c|c} \Gamma_f & \Gamma_s \Delta_k \\ \hline 0 & I \;\; \Delta_k \end{array}\right] \begin{bmatrix} \underline{u}_{f_k} \\ \hline \underline{v}_k \end{bmatrix} \qquad (2.3\text{-}5)$$

where:

$$\Delta_k = \begin{bmatrix} \delta_{k,i_1\ell_1} & & 0 & \cdots & 0 \\ & \ddots & & & \vdots \\ 0 & & \delta_{k,i_2\ell_2} & & \vdots \\ \vdots & & & \ddots & \vdots \\ 0 & \cdots & 0 & 0 & \delta_{k,i_{m'}\ell_{m'}} \end{bmatrix} \qquad (2.3\text{-}6)$$

where m' is the dimension of $\underline{v}$ and

$$\delta_{k,i_j\ell_j} = \begin{cases} 1; i_j\ell_j = k \\ 0; i_j\ell_j \neq k \end{cases} \qquad (2.3\text{-}7)$$

The matrix Δ_k is a generalization of the Kronecker delta functions used in the two-sample-rate case. Each diagonal element of Δ_k nulls the input to a particular low rate control holding circuit on cycles between new computations of that control. For example, if u_{s2} is computed every two cycles (i.e., $\ell_2 = 2$) then the second diagonal element of Δ_k will be zero on cycles when k is not a multiple of two (i.e., $k \neq i_2\ell_2$). A set of periodic regulator gains for a representative flight control system and an analysis of the performance of that system are presented in Section 2.5.

2.3.2 Multirate Regulator Design Procedure

The multirate regulator is designed through the following procedure:

(1) A continuous-time regulator is designed to meet continuous-time performance specifications

(2) Discrete-time regulator weighting matrices for the single rate case are derived from those used to design the continuous-time regulator

(3) The discrete-time periodic weighting matrices used to solve for the multirate gains are constructed from the single rate matrices. The multirate gains are derived from the periodic steady-state solution of the discrete-time Ricatti equation.

The first step involves the normal iterative design process associated with designing an optimal regulator; i.e., trial and error assignment of weighting matrix elements to yield a regulator that meets the design specifications. The relationships presented by Gran, Berman, and Rossi (Ref. 5) are then used to

compute the single-rate (i.e., fast rate) discrete-time weighting matrices from the continuous-time matrices. Using the augmented system representation, Eq. 2.3-2, and the relationships in Ref. 5, expressions are derived for the multirate weighting matrices; inspection of these expressions indicates that the multirate matrices can be constructed from the single-rate matrices computed in step (2) above. An implicit benefit of this three-step approach is that the performance of the continuous-time, single-rate discrete-time, and multirate discrete-time controllers can be compared on a one-to-one basis; i.e., each control design is based on optimizing the same continuous-time cost functional (Ref. 5).

The first step of the design process uses the continuous-time representation of the plant dynamics and an infinite-time-horizon quadratic cost functional:

$$\dot{\underline{x}} = F\underline{x} + G\underline{u} \tag{2.3-8}$$

$$J = \frac{1}{2}\int_0^\infty (\underline{x}^T Q\underline{x} + \underline{u}^T R\underline{u})dt \tag{2.3-9}$$

Regulator gains, C, are derived by solving the time-invariant form of the continuous Ricatti equation:

$$0 = PF + F^T P + Q - PGR^{-1}G^T P \tag{2.3-10}$$

$$C^T = -R^{-1}G^T P \tag{2.3-11}$$

The designer chooses the Q and R matrices of the cost functional such that the derived closed-loop system:

$$\dot{\underline{x}} = (F + GC^T)\underline{x} + G\underline{u} \qquad (2.3\text{-}12)$$

meets desired design specifications.

The second-step of the design process, the derivation of equivalent single-rate discrete-time weighting matrices, uses the discrete representation of the plant dynamics and cost functional:

$$\underline{x}_{k+1} = \Phi\underline{x}_k + \Gamma\underline{u}_k \qquad (2.3\text{-}13)$$

$$J = \frac{1}{2}\sum_{k=0}^{\infty}(\underline{x}_k^T\bar{Q}\underline{x}_k + 2\underline{x}_k^T\bar{M}\underline{u}_k + \underline{u}_k^T\bar{R}\underline{u}_k) \qquad (2.3\text{-}14)$$

Discrete regulator gains are derived by propagating the discrete Ricatti equation to steady-state; i.e., propagate:

$$\bar{L}_k = (\Gamma^T\bar{P}_{k+1}\Gamma + \bar{R})^{-1}\Gamma^T\bar{P}_{k+1} \qquad (2.3\text{-}15)$$

$$\bar{P}_k = \theta^T(I - L_k^T\Gamma^T)\bar{P}_{k+1}\theta + Q^* \qquad (2.3\text{-}16)$$

where

$$\theta \equiv \Phi - \Gamma\bar{R}^{-1}\bar{M}^T \qquad (2.3\text{-}17)$$

$$Q^* \equiv \bar{Q} - \bar{M}\bar{R}^{-1}\bar{M}^T \qquad (2.3\text{-}18)$$

The control gains in steady-state are:

$$\bar{C} = \bar{R}^{-1}\bar{M}^T + L\theta \qquad (2.3\text{-}19)$$

The weighting matrices -- $\overline{Q}$, $\overline{M}$, and $\overline{R}$ -- that yield a discrete cost functional equivalent to the continuous cost functional, Eq. 2.3-9, are derived from the following expressions (Ref. 5):

$$Q = \int_0^{T_s} \Phi^T(t,0)\, Q\, \Phi(t,0)dt \qquad (2.3\text{-}20)$$

$$M = \int_0^{T_s} \Phi^T(t,0)\, Q\, \Gamma(t,0)dt \qquad (2.3\text{-}21)$$

$$R = T_s R + \int_0^{T_s} \Gamma^T(t,0)\, Q\, \Gamma(t,0)dt \qquad (2.3\text{-}22)$$

where

$$\Phi(t,0) = e^{Ft}$$

$$\Gamma(t,0) = \int_0^t e^{F\tau} G\, d\tau$$

Finally, the <u>third step</u> is the design of the multirate system. Again, the two-sample-rate case will be described first; extension to the multirate case is straightforward and will be described later in this section. The discrete representation of the plant dynamics augmented by the slow control holding circuit states is repeated here along with the cost functional. Note that the weighting matrices of the cost functional are time-varying, i.e., $\hat{Q}_k$, M_k, $\hat{R}_k$. In the present formulation, the dimensions of M_k and R_k vary according to the number of controls that are computed on cycle k. The augmented control effectiveness matrix, $\hat{\Gamma}_k$, is time-varying due to the presence of the Kronecker delta's; on cycles when $\underline{v}_k$ is not computed the zero columns of $\hat{\Gamma}_k$ are deleted, thereby reducing its column order. Also, $\underline{v}_k$ is included in the $\tilde{\underline{u}}_k$ vector only

on cycles when a new value of $\underline{v}_k$ is computed; on all other cycles $\underline{v}_k$ is deleted.

$$\begin{bmatrix} \underline{x}_{k+1} \\ \hline \underline{u}_{s_{k+1}} \end{bmatrix} = \left[\begin{array}{c|c} \Phi & \Gamma_s \\ \hline 0 & I \end{array}\right] \begin{bmatrix} \underline{x}_k \\ \hline \underline{u}_{s_k} \end{bmatrix} + \left[\begin{array}{c|c} \Gamma_f & \Gamma_s \delta_{k,i\ell} \\ \hline 0 & I\ \delta_{k,i\ell} \end{array}\right] \begin{bmatrix} \underline{u}_{f_k} \\ \hline \underline{v}_k \end{bmatrix} \tag{2.3-23}$$

$$= \tilde{\Phi}\tilde{\underline{x}}_k + \hat{\Gamma}_k\tilde{\underline{u}}_k \tag{2.3-24}$$

$$J = \frac{1}{2}\sum_{k=0}^{\infty}\left\{(\underline{x}_k^T\ \underline{u}_{s_k}^T)\ \hat{Q}_k \begin{pmatrix} \underline{x}_k \\ \hline \underline{u}_{s_k} \end{pmatrix} + 2(\underline{x}_k^T\ \underline{u}_{s_k}^T)\ \hat{M}_k\tilde{\underline{u}}_k + \tilde{\underline{u}}_k^T\hat{R}_k\tilde{\underline{u}}_k\right\} \tag{3.2-25}$$

Discrete multirate regulator gains are derived by propagating the discrete Ricatti equation to periodic steady state:

$$\hat{L}_k = (\hat{\Gamma}_k^T\hat{P}_{k+1}\hat{\Gamma}_k + \hat{R}_k)^{-1}\ \hat{\Gamma}_k^T\hat{P}_{k+1} \tag{2.3-26}$$

$$\hat{P}_k = \hat{\theta}_k^T(I - \hat{L}_k^T\hat{\Gamma}_k^T)\hat{P}_{k+1}\hat{\theta}_k + \hat{Q}_k^* \tag{2.3-27}$$

where:

$$\hat{\theta}_k = \hat{\Phi} - \hat{\Gamma}_k\hat{R}_k^{-1}\hat{M}_k^T \tag{2.3-28}$$

$$\hat{Q}_k^* = \hat{Q}_k - \hat{M}_k\hat{R}_k^{-1}\hat{M}_k^T \tag{2.3-29}$$

The control gains over one complete period are:

$$\hat{C}_i = \hat{R}_i^{-1}\hat{M}_i^T + \hat{L}_i\hat{\theta}_i \quad ; \quad i=0,1,2,\ldots\ell-1 \tag{2.3-30}$$

It is desired to find $\hat{Q}_k$, $\hat{M}_k$, and $\hat{R}_k$ such that the cost functional of the multirate system design is equivalent to that of the continuous system, Eq. 2.3-9. The procedure to find the discrete multirate weighting matrices is, again, to use the weighting matrices of the continuous system and the relationships in Ref. 5 to derive the discrete-time matrices.

Augmentation of the plant dynamics by the slow control holding circuit states requires modification of the continuous-time weighting matrices. The somewhat involved mathematical procedure associated with modifying the continuous-time matrices and deriving the discrete-time matrices from them is covered in Appendix A; the weighting matrices for the discrete-time multirate design are summarized here:

$$\hat{Q}_k = \left[\begin{array}{c|c} \bar{Q} & \bar{M}_s \\ \hline \bar{M}_s^T & \bar{R}_s \end{array}\right] \tag{2.3-31}$$

On cycles when all controls are updated (i.e., $k = i\ell$):

$$\hat{R}_{i\ell} = \bar{R} \tag{2.3-32}$$

$$\hat{M}_{i\ell} = \left[\begin{array}{c} \bar{M} \\ \hline \bar{R}_{sf} \quad \bar{R}_s \end{array}\right] \tag{2.3-33}$$

On all other cycles (i.e., $k \neq i\ell$):

$$\hat{R}_k = \bar{R}_f \tag{2.3-34}$$

$$\hat{M}_k = \begin{bmatrix} \bar{M}_f \\ \hline \bar{R}_{sf} \end{bmatrix} \tag{2.3-35}$$

where the f- and s-partitions have dimensions corresponding to the number of fast and slow controls, respectively. The result that the multirate matrices can be constructed from the single rate matrices is very fortunate since software packages to compute the single-rate matrices are already in common usage. Again, the multirate regulator derived from these matrices optimizes the same cost function (defined in continuous-time) as the single-rate and continuous-time designs.

Derivation of the cost functional weighting matrices for the general multirate case (i.e., more than two sample rates) is accomplished by using the dynamics given by Eq. 2.3-5 and the relationships from Ref. 5. Again, the derivation is presented in Appendix A; the results of this derivation are:

$$\hat{Q}_k = \begin{bmatrix} \bar{Q} & \bar{M}_s \\ \hline \bar{M}_s^T & \bar{R}_s \end{bmatrix} \tag{2.3-36}$$

$$\hat{R}_k = \begin{bmatrix} \bar{R}_f & \bar{R}_{sf}^T \Delta_k \\ \hline \Delta_k \bar{R}_{sf} & \Delta_k \bar{R}_s \Delta_k \end{bmatrix} \tag{2.3-37}$$

$$\hat{M}_k = \begin{bmatrix} \bar{M}_f & \bar{M}_s \Delta_k \\ \hline \bar{R}_{sf} & \bar{R}_s \Delta_k \end{bmatrix} \tag{2.3-38}$$

The presence of the Δ_k's causes appropriate rows and columns of the $\hat{R}_k$ and $\hat{M}_k$ matrices to be set to zero on cycles between new computations of the slow controls. In introducing these cost functional matrices into the discrete-time Ricatti equation there is a choice in dealing with the zero rows and

columns: they can be deleted, thereby reducing the order of $\hat{R}_k$ and $\hat{M}_k$ (this was done in the two-sample-rate development) or they can be retained with certain computational provisions. If the zero rows and columns are retained a question arises in the computation of $\hat{L}_k$, i.e.:

$$\hat{L}_k = (\hat{\Gamma}_k^T \hat{P}_{k+1} \hat{\Gamma}_k + \hat{R}_k)^{-1} \hat{\Gamma}_k^T \hat{P}_{k+1} \qquad (2.3\text{-}39)$$

If the zero rows and columns of $\hat{\Gamma}_k$ and $\hat{R}_k$ are retained, the matrix, $\hat{\Gamma}_k^T \hat{P}_{k+1} \hat{\Gamma}_k + \hat{R}_k$, has zero rows and columns and, therefore, is not explicitly invertable. If it is recognized, however, that certain rows $\hat{L}_k$ are constrained to be zero (i.e., those rows corresponding to control increments not computed on cycle k), the invertability problem can be resolved. If the singular value decomposition method is used in the matrix inversion of Eq. 2.3-39 the rows of $\hat{L}_k$ corresponding to control increments not computed on cycle k will be zero; the nonzero rows of $\hat{L}_k$ will be identical to those that would be computed by deleting the zero rows and columns of $\hat{\Gamma}_k$ and $\hat{R}_k$.

2.4 EIGENVALUE-EIGENVECTOR ANALYSIS OF MULTIRATE SYSTEMS

A methodology for frequency domain evaluation of digital multirate control systems is described in this section. This technique is based on an extension of the single-rate control system analysis method presented in Ref. 7.

It is known that a single-rate time-invariant discrete-time system has stable dynamics if the eigenvalues of that system all lie within the unit semicircle of the complex plane. The stability of a multirate system can be determined in a similar manner; it is necessary, however, to consider the dynamics of the system over an entire control period.

Consider the state propagation of a closed-loop multirate control system:

$$\tilde{\underline{x}}_{k+1} = \hat{\Phi}_k \tilde{\underline{x}}_k + \hat{\Gamma}_k \tilde{\underline{u}}_k \qquad (2.4\text{-}1)$$

$$= (\hat{\Phi}_k - \hat{\Gamma}_k \hat{C}_k) \tilde{\underline{x}}_k \qquad (2.4\text{-}2)$$

where $\hat{\Gamma}_k$ and $\hat{C}_k$ are periodic. The stabilizing effects of the multirate controls can be assessed by determining the state propagation over a complete multirate control cycle; i.e., using Eq. 2.4-2 recursively, the state transition over ℓ subinterval cycles can be derived:

$$\tilde{\underline{x}}_{k+\ell} = \left[\prod_{i=1}^{\ell} (\hat{\Phi}_{(k+\ell)-i} - \hat{\Gamma}_{(k+\ell)-i} \hat{C}_{(k+\ell)-i}) \right] \tilde{\underline{x}}_k \qquad (2.4\text{-}3)$$

$$= \Phi_* \tilde{\underline{x}}_k \qquad (2.4\text{-}4)$$

Here Φ_* represents the closed loop dynamics of the multirate control system over a complete control cycle. The stability and, to a limited extent, the transient response characteristics of the system are determined by the eigenvalues of Φ_*. Note that the sample period associated with this stability analysis is ℓT_s, the period of the complete control cycle.

An alternative frequency domain interpretation of the multirate system dynamics is possible by determining the continuous-time equivalent (Ref. 7) of Φ_*, i.e.:

$$F_* = \frac{1}{\ell T_s} \ell n \, \Phi_* \qquad (2.4\text{-}5)$$

Here the matrix natural logarithm is defined by the series expansion:

$$\ell n\Phi = [(\Phi - I) - \frac{1}{2}(\Phi - I)^2 + \frac{1}{3}(\Phi - I)^3 + \ldots] \tag{2.4-6}$$

Having computed F_*, continuous-time eigenvalues equivalent to those of Φ_* can be obtained from the determinant:

$$|\lambda I - F_*| = 0 \tag{2.4-7}$$

The eigenvectors, $\underline{x}_i'$, corresponding to the distinct roots of Eq. 2.4-7, λ_i, are determined by the nontrivial solution of Eq. 2.4-8.

$$F_*\underline{x}_i' = \lambda_i \underline{x}_i' \tag{2.4-8}$$

If control specifications are given in terms of real frequency domain criteria (i.e., bandwidth, damping ratio) the methodology of this section can be used to translate the multirate digital system characteristics into the real frequency domain. The commonly used analysis methods such as root-locus are also possible by this transformation.

2.5 EXAMPLE MULTIRATE SYSTEM

The properties and performance of a multirate optimal regulator/estimator flight control system are described in this section. The plant to be used in this example is the linearized lateral dynamics of the Space Shuttle Orbiter during reentry; the details of this model are included in Appendix B.

2.5.1 Plant/Measurement Description

The plant to be controlled is the linearized lateral dynamics of the Space Shuttle Orbiter during reentry. A discrete-time representation based on a fast sample rate of 6.25 Hz* is adopted:

$$\underline{x}_{k+1} = \Phi\, \underline{x}_k + \Gamma_f \delta_{a_k} + \Gamma_s \delta_{r_k} + \Lambda \underline{w}_k \qquad (2.5\text{-}1)$$

$$\underline{x}_k^T = (v,\ r_b,\ p_b,\ \phi)_k \qquad (2.5\text{-}2)$$

$$= \text{(sideslip velocity, yaw rate, roll rate, roll angle)}$$

$$\delta_a = \text{aileron deflection} \qquad (2.5\text{-}4)$$

$$\delta_r = \text{rudder deflection} \qquad (2.5\text{-}5)$$

$$\underline{w}_k = \text{white noise turbulence} \qquad (2.5\text{-}6)$$

$$E\{\Lambda \underline{w}_k \underline{w}_k^T \Lambda^T\} = Q \qquad (2.5\text{-}7)$$

The values of the various system matrices: Φ, Γ_f, Γ_s, Λ, and Q are presented in Appendix B.

The measurements available to the estimation/control system are shown in Fig. 2.5-1. Three of the four measurements: roll rate, yaw rate, and lateral acceleration are sampled at 6.25 Hz; the stable platform yields an explicit measurement of roll angle, ϕ, at 0.25 Hz.

*The sample rate used in the operational space shuttle control system is 25 Hz. The lower sample rate of 6.25 Hz was chosen for this example to accentuate the periodic nature of the multirate estimation and control system.

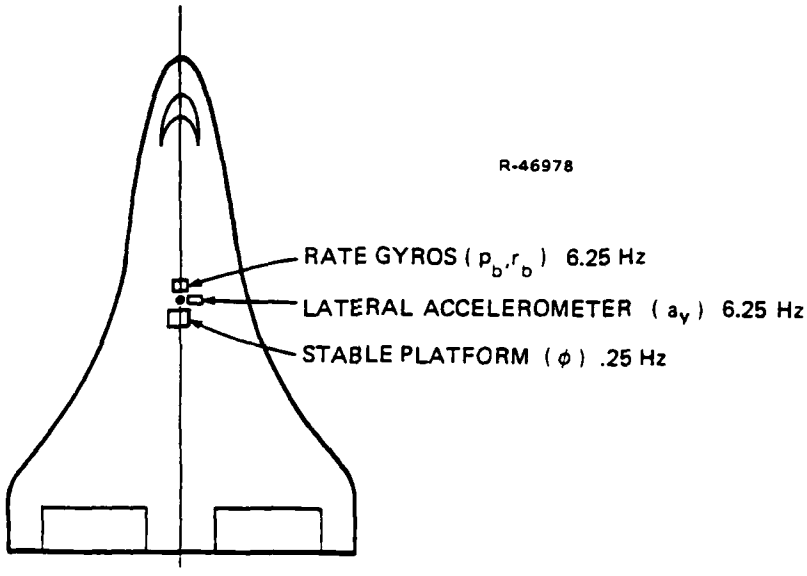

Figure 2.5-1 Vehicle Instrumentation

2.5.2 Multirate Kalman Filter Design

Mathematically, the system measurements are described by:

$$\underline{z}_{f_k} = H_f \underline{x}_k + \underline{v}_{f_k} \quad ; \text{ all } k \qquad (2.5\text{-}8)$$

= (lateral accelerometer, yaw rate gyro, roll rate gyro) (2.5-9)

$$z_{s_k} = H_s \underline{x}_k + v_{s_k} \quad ; \; k = i\ell \qquad (2.5\text{-}10)$$

= (Inertial Navigation System [INS] roll angle measurement) (2.5-11)

with:

$$\ell = 25 \tag{2.5-12}$$

H_f = matrix of lateral accelerometer, roll and yaw rate gyro sensitivities (2.5-13)

H_s = INS roll angle sensitivity (2.5-14)

$\underline{v}_{f_k}$ = vector of accelerometer, roll and yaw gyro noises (zero mean) (2.5-15)

v_{s_k} = INS noise (zero mean) (2.5-16)

The measurement noise statistics are described by:

$$E\left\{\underline{v}_{f_k}\ \underline{v}_{f_k}^T\right\} = R_f \quad ; \ k \neq i\ell \tag{2.5-17}$$

$$E\left\{\begin{pmatrix}\underline{v}_{f_k}\\ \hline v_{s_k}\end{pmatrix}\left(\underline{v}_{f_k}^T \quad v_{s_k}\right)\right\} = \left[\begin{array}{c|c} R_f & 0 \\ \hline 0 & R_s \end{array}\right] \quad ; \quad k = i\ell \tag{2.5-18}$$

The numerical values of the H and R matrices are presented in Appendix B.

The periodically varying H- and R-matrices and the Φ- and Q-matrices are used to propagate Eqs. 2.2-10 through 2.2-13 to periodic steady-state. The periodic steady-state Kalman gains are then used to implement the following state estimator:

$$\hat{\underline{x}}_{k+1} = \Phi\hat{\underline{x}}_k + K_{f_k}\left(\underline{z}_{f_{k+1}} - H_f\Phi\hat{\underline{x}}_k\right) \quad ; \ k \neq i\ell \tag{2.5-19}$$

$$\hat{\underline{x}}_{k+1} = \Phi\hat{\underline{x}}_k + \begin{bmatrix} K_f & K_s \end{bmatrix}\left[\begin{pmatrix} \underline{z}_f \\ \hline \underline{z}_s \end{pmatrix}_{k+1} - \begin{pmatrix} H_f \\ \hline H_s \end{pmatrix}\Phi\hat{\underline{x}}_k\right] \quad (2.5\text{-}20)$$

$$; \; k = i\ell$$

The state estimator yields the optimal estimates of sideslip velocity, yaw rate, roll rate, and roll angle using the available instruments and the specified sample rates.

The operation of the state estimator can be described heuristically. On cycles when all four measurements are available, the yaw rate gyro, roll rate gyro, and INS roll angle measurements are low-pass filtered (to reject measurement noise) to produce estimates of yaw rate, roll rate, and roll angle; a linear combination of the lateral accelerometer output and the output of the other three instruments is low-pass filtered to yield an estimate of sideslip velocity. On cycles when the INS measurement is not available, roll angle is estimated (extrapolated) by integrating the roll rate gyro output (this integration is implicit in the state transition matrix, Φ). Every 25th cycle the roll angle estimate is "reset" via the INS measurement; on subsequent cycles the extrapolation process is repeated.

On cycles when the roll angle is being extrapolated, roll rate gyro measurement residuals are used to improve the roll angle estimate. Figure 2.5-2 shows the history of the roll rate gyro to roll angle gain, K_{43}, over time. On cycle 0, the INS roll angle measurement is available and K_{43} has a very small value; i.e., when the INS measurement is available, the rate gyro measurement is ignored in estimating ϕ. On cycles following the INS measurement K_{43} assumes larger values; i.e., as the number of cycles since the last INS measurement increases

the estimator relies more and more on roll rate gyro residuals to generate the estimate of ϕ. On cycle 25, the INS measurement is again available and K_{43} is set to the same small value it had on cycle 0.

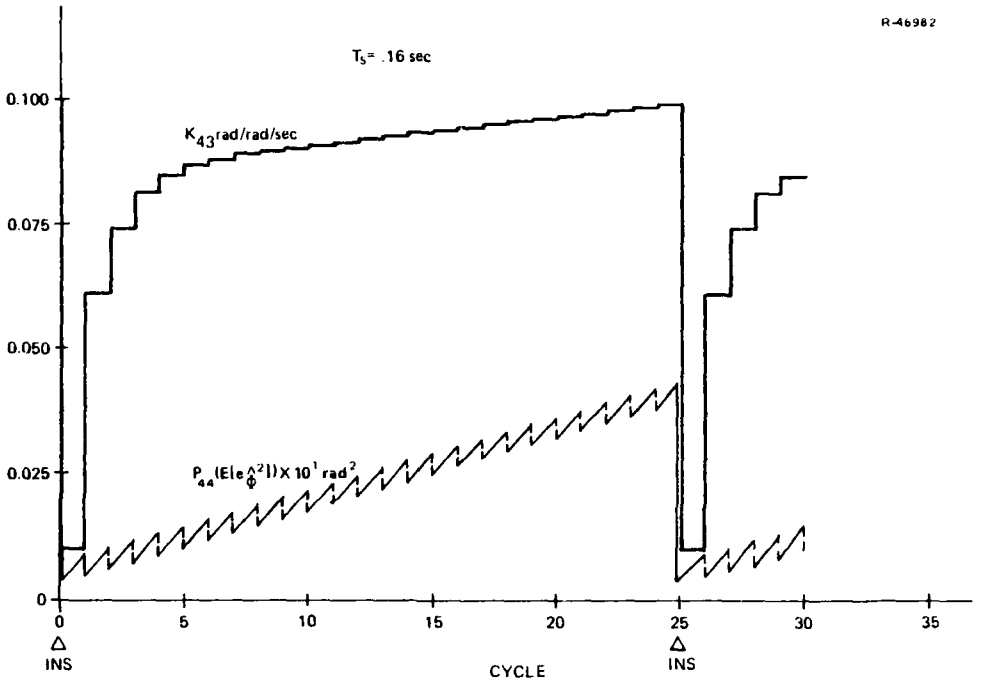

Figure 2.5-2 Roll Rate Gyro to Roll Angle Gain of Example Estimator

Also shown in Fig. 2.5-2 is the evolution of the roll angle estimation error covariance, P_{44}. On cycle 0 the estimation error is small; an INS measurement has provided an accurate estimate of ϕ. On cycles follwing cycle 0, the extrapolation of ϕ using the roll rate gyro causes the estimation error variance to grow; i.e., although an optimal estimate is being produced, this estimate drifts away from the true value. The "saw-tooth" nature of the error covariance curve indicates that some improvement of the estimation error is achieved on each cycle through use of the roll rate gyro residuals (i.e.,

the estimation error drops following the measurement). On cycle 25 the estimation error is reset using the INS measurement.

2.5.3 Multirate Regulator Design

The goal of the multirate regulator design is to determine the multirate regulator that is equivalent to an existing continuous-time (analog) regulator. The specifications of the continuous-time regulator in terms of its closed-loop eigenvalues are:

Roll-Spiral Dynamics:

$$s = -0.632 \pm i\ 0.913\ (\omega_o = 1.11 \text{ rad/sec}, \xi = 0.569) \tag{2.5-21}$$

Dutch Roll Dynamics:

$$s = -0.522 \pm i\ 0.159\ (\omega_o = 0.546 \text{ rad/sec}, \xi = 0.957) \tag{2.5-22}$$

The continuous-time control and state weighting matrices, R and Q, used to design the continuous-time regulator are presented in Appendix B.

A sample rate of 6.25 Hz is chosen for the aileron control computations. The rudder control, which is used to damp the dutch-roll mode, is computed at 1.56 Hz (i.e., 6.25 Hz/4.); since the closed-loop dutch-roll mode has a damped frequency that is roughly one-sixth the frequency of the roll-spiral mode, 1.56 Hz is a reasonable sample rate for the rudder computations.

Using the system dynamics, Eq. 2.5-1, and the $\overline{Q}$ and $\overline{R}$ matrices corresponding to the continuous-time regulator, the single-rate (6.25 Hz) discrete-time weighting matrices, $\overline{Q}$, $\overline{R}$, and $\overline{M}$, are computed using Eqs. 2.3-20 through 2.3-22. The periodically time-varying weighting matrices, $\hat{Q}_k$, $\hat{R}_k$, and $\hat{M}_k$, are constructed from the appropriate single-rate weighting matrix partitions using Eqs. 2.3-31 through 2.3-35.

The vehicle dynamics augmented by the rudder control holding circuit are given by:

$$\begin{bmatrix} \underline{x}_{k+1} \\ \hline \delta_{r_{k+1}} \end{bmatrix} = \left[\begin{array}{c|c} \Phi & \Gamma_s \\ \hline 0 & I \end{array}\right] \begin{bmatrix} \underline{x}_k \\ \hline \delta_{r_k} \end{bmatrix} + \left[\begin{array}{c|c} \Gamma_f & \Gamma_s \delta_{k,i\ell} \\ \hline 0 & \delta_{k,i\ell} \end{array}\right] \begin{bmatrix} \delta_{a_k} \\ \hline v_{r_k} \end{bmatrix} \tag{2.5-23}$$

Using the dynamics described by Eq. 2.5-23 and the multirate weighting matrices ($\hat{Q}_k$, $\hat{R}_k$, $\hat{M}_k$), Eqs. 2.3-26 and 2.3-27 are propagated to periodic steady-state. The periodic gains $\hat{C}_i$ are computed by Eq. 2.3-30; Fig. 2.5-3 shows the values of the periodic aileron gains along with the corresponding single-rate (6.25 Hz) gains. The values of roll rate and roll angle to aileron gains, C_{13} and C_{14} are essentially constant over the four cycle control period, and are equal to the single rate gains. This similarity of the single rate and multirate gains involving roll dynamics and aileron control is not surprising; roll control is the natural inner loop of a lateral control system (i.e., the dynamics which dictate the highest sample rate). The lateral acceleration, yaw rate, and slow control crossfeed gains (C_{11}, C_{12}, and C_{sf}, respectively) vary significantly over the control period, assuming values closest to the single rate values on cycles when a new rudder control is computed (cycles 0 and 4). The variations of C_{11}, C_{12}, and

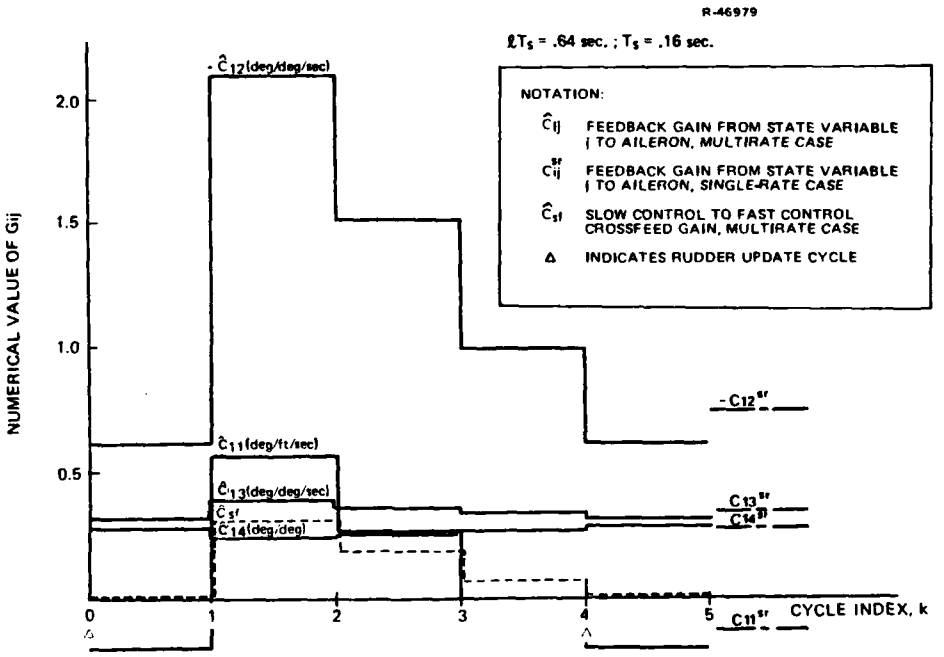

Figure 2.5-3 Multirate Regulator Aileron Gains

C_{sf} over the control cycle indicate that the optimal control design uses the aileron partially to compensate lateral acceleration and yaw (which are normally compensated by the rudder) between rudder updates.

It should be noted that variations of the fast control gains over the control period are a result that is unique to the present synthesis techniques; classical analysis techniques and commonly used ad-hoc design methods (such as Tustin transform) are restricted to constant gains. Optimality of the present design indicates that restriction of multirate gains

to constant values (as is done in the classical approaches) precludes an optimal or near-optimal control design.

2.5.4 System Performance

The performance of the multirate estimation/control system is evaluated in three steps:

- Comparison of the multirate estimator error variances with those of a multi-rate estimator which uses gains derived from a single-rate design
- Comparison of the multirate regulator transient response with that of the continuous-time system used to derive the multirate design
- Comparison of the error rejection variances of the multirate estimation/control system with those of a multirate system which uses estimation and control gains derived from a single-rate design

The estimation/control design used for comparison with the multirate design indicates the type of system that would result if the present multirate design technique were not available; i.e., the designer would derive the gains for the single-rate (fast rate) case, then simply implement these gains in a multi-rate structure as a first approximation. As the comparisons will show, the multirate system designed by the present technique clearly out-performs this single-rate based system.

Estimator Performance - Table 2.5-1 shows the estimation error variances for the optimal multirate filter and the single-rate based multirate estimator derived from time-domain simulation (i.e., a single monte-carlo replication of each system). As the values indicate, v, r_b, and p_b are estimated with essentially

equal accuracy by both estimators (small differences in the estimation errors of the two filters are attributable to the fact that only a single replication of each system was performed); this is not surprising since in both estimators, v, r_b, and p_b are generated by effectively low pass filtering and forming linear combinations of (fast sample rate) accelerometer and rate gyro measurements. The optimal multirate filter clearly estimates roll angle more accurately than the single-rate based filter. Superior roll angle estimation is also expected since the optimal multirate design makes best use of roll rate gyro residuals between INS updates (recall the variation of the roll rate gyro to roll angle gain in Fig. 2.5-3); the single-rate design uses roll rate gyro residuals incorrectly in a multirate implementation.

TABLE 2.5-1
ESTIMATION ERROR VARIANCES

VARIABLE / SYSTEM	v (ft^2/sec^2)	r_b (deg^2/sec^2)	p_b (deg^2/sec^2)	ϕ(deg^2)
Optimal Multirate	8.282	0.1347	0.1561	0.2619
Single Rate Design	9.081	0.1347	0.1336	0.5107

Regulator Transient Response - Figure 2.5-4 shows the desired closed-loop system transient response to an initial roll rate error of 1 deg/sec (represented by the "continuous system" response). As the (digitized) multirate design response indicates, the transient responses of the continuous and multi-rate systems are very similar. Also shown in Fig. 2.5-4 is the closed-loop system response that would result by using

regulator gains from a single-rate design in a multirate formulation. The single-rate based system lags the desired response significantly; as Fig. 2.5-5 shows, this lag generates a sizeable overshoot of roll angle during the transient.

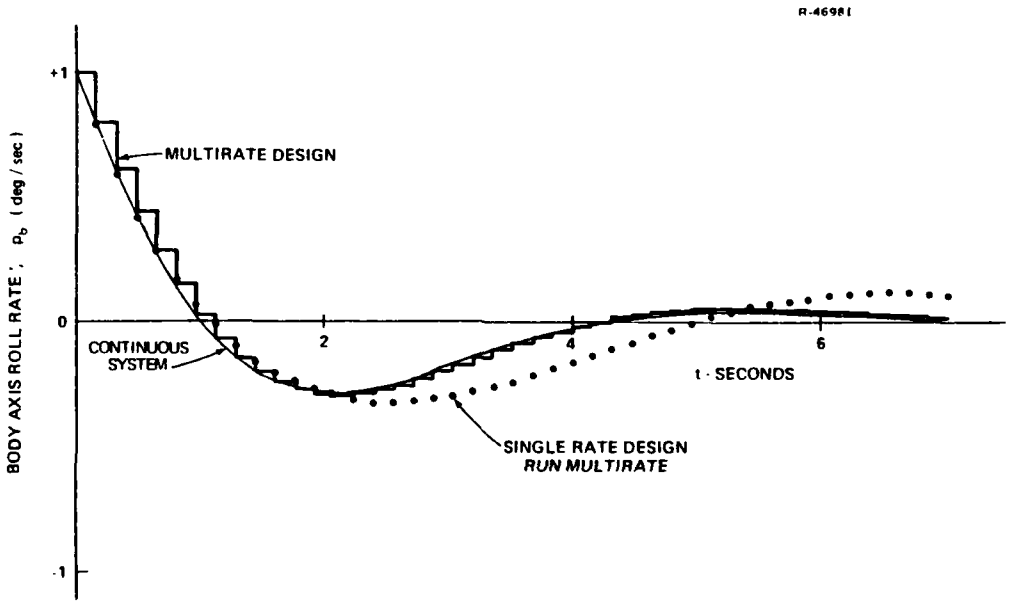

Figure 2.5-4 Roll Rate Responses to Initial Roll Rate Error

Estimation/Control System Stabilization Effectiveness - The ability of the combined estimation/control system to reject disturbances (as characterized by the process noise matrix Q defined by Eq. 2.5-7) is summarized in Table 2.5-2. For comparison, the performance of a multirate estimation/control system based on single-rate design (i.e., the single-rate estimator and controller described in the estimation error and transient response comparisons of this section) is also presented. The RMS values in Table 2.5-2 indicate that roll attitude and sideslip velocity are regulated far better by the

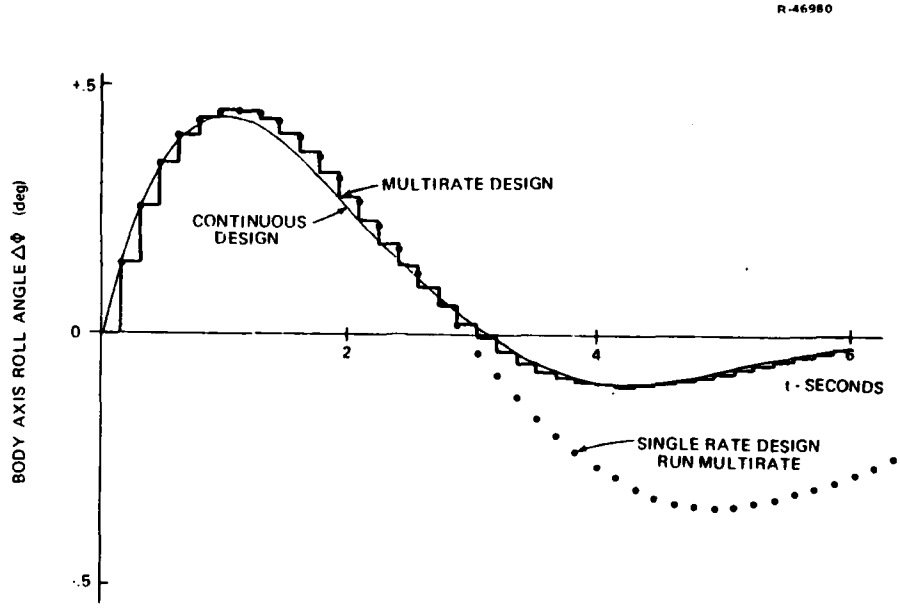

Figure 2.5-5 Roll Angle Responses to Initial Roll Rate Error

TABLE 2.5-2
COMBINED ESTIMATION/CONTROL SYSTEM RMS STATE ERROR

VARIABLE / SYSTEM	v(ft/sec)	r_b(deg/sec)	p_b(deg/sec)	φ(deg)
Optimal Multirate	6.50	4.83	22.5	37.2
Single Rate Design	11.50	4.64	21.8	66.0

optimal multirate system than with the single-rate based design while essentially equal yaw rate and roll rate regulation is achieved by both systems (again, slight differences in yaw rate and roll rate RMS are attributable to the fact that a single monte-carlo replication of each system was used to generate the data). Improved roll angle regulation from the multirate system should be expected since the optimal multirate estimator generated significantly more accurate estimates than the single-rate based estimator (Table 2.5-1).

2.6 CHAPTER SUMMARY

Formulation and mathematical solution of the multirate estimation and control problem for the case of two sample rates have been presented. The filter synthesis technique described in this chapter yields the optimal state estimator for a given set of instruments and measurement data rates; the control design technique determines the multirate regulator that optimizes the same cost functional as that used to design a specified continuous-time regulator.

Our multirate estimator design approach is characterized by a set of periodic gains which make best use of measurement residuals between major updates (i.e., cycles when all measurements are available). In an example aircraft application, a multirate estimator design yielded a significant reduction in roll attitude estimation error through the use of roll rate gyro residuals between INS updates.

The multirate control formulation requires augmentation of the system dynamic model by holding circuit dynamics corresponding to controls that are computed at slow rates. The multirate control design consists of sets of periodically varying

feedback gains plus a crossfeed path from the low sample rate control channel to the high rate channel. Periodic variations of the high rate control gains indicate that the high rate controls partially compensate dynamics normally handled by the slow controls between slow control updates.

Again, state estimators and controllers designed by the present technique are the optimal designs. The periodically time-varying gains which characterize the optimal designs are a unique product of the present technique; classical analysis techniques and commonly used ad-hoc design methods (such as Tustin transform) are restricted to constant gains. Optimality of the present designs indicates that restriction of multirate gains to constant values (as is done in the classical approaches) precludes an optimal or near-optimal design.

The present multirate synthesis techniques simplify the design process significantly. It is possible to design a controller in continuous-time to meet desired specifications then derive an equivalent multirate digital design through a direct, straightforward mathematical procedure. Design by classical analysis techniques would require an educated trial-and-error process to generate an acceptable multirate system.

3. MULTIRATE PROPORTIONAL PLUS INTEGRAL CONTROL

3.1 OVERVIEW

The basic regulator control structure is appropriate in applications where it is desired to drive the plant state to zero in an optimal manner. The regulator is also useful in situations where a prescribed state trajectory is to be followed or the plant state is to be stabilized about a state trajectory generated by a feedforward controller. In all of the regulator applications described here, it is assumed that the dynamics of the plant and of all plant input commands and disturbances are accurately known; if the plant or disturbance dynamics are not known precisely, inadequate performance can result. For example, if it is desired to regulate a plant about a step input command, any mismatch between the dynamic model used to design the regulator and the true dynamics will result in a steady-state error of the plant output.

In most practical situations, the dynamics of the plant are not precisely known and disturbances to the plant cannot be characterized a priori. Uncertainty of the plant and its disturbance environment is very common in flight vehicle control; one usually has only approximate knowledge of the vehicle aerodynamics, the flight condition of the vehicle, and the state of atmospheric turbulence. In addition, it is desired that the vehicle follow nonzero input commands with zero steady state error; e.g., follow a nonzero bank angle command to make a turn.

In applications where plant and disturbance uncertainties must be accommodated effectively, control structures having an integral feedback path are appropriate. Figure 3.1-1 shows the structure of the proportional-plus-integral controller. In addition to a feedback control proportional to the state $\underline{u}_p$ (i.e., proportional path) the error between the plant output $\underline{y}$ and the desired output $\underline{y}_d$ is integrated to compute $\underline{u}_i$. For a constant value of $\underline{y}_d$, the controls $\underline{u}_p$ and $\underline{u}_i$ have constant values in steady state; a constant value of $\underline{u}_i$ implies that the output error, $\underline{y}_d$-$\underline{y}$, has been driven to zero. This very desirable property of zero steady-state error to a constant command is maintained even when there is a mismatch of the plant design model and the true plant dynamics; the integrating action of the controller ensures that the error is driven to zero. The PI control structure has been used with success in several flight control applications (Ref. 7, 8 and 9).

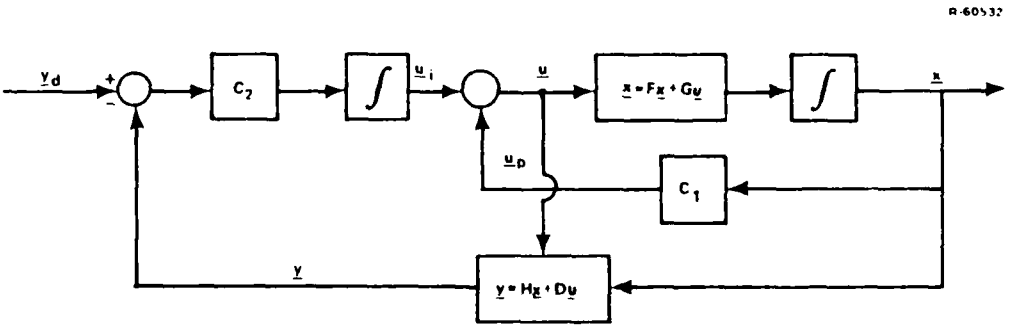

Figure 3.1-1 Proportional-Plus-Integral Control

The principles of optimal multirate regulator theory developed in Section 2.3 are extended to the proportional-plus-integral (PI) control structure in this chapter. Two alternative PI control structures are developed: one in which

a standard zero-order-hold function is used to output the computed controls and another in which slow controls are smoothed by "staircasing" them between updates. The PI controller formulations are applied to a design example, a command augmentation system for the F-14 aircraft; the closed-loop properties of the multirate controller are compared to those of an equivalent single-rate controller.

The organization of this chapter is as follows: the multirate proportional-plus-integral structures are developed in Section 3.2. One of the PI structures is applied to a design example in Section 3.3, and the controller properties and transient response characteristics of the example are also described. The chapter is summarized in Section 3.4.

3.2 FORMULATION OF THE PROPORTIONAL-PLUS-INTEGRAL CONTROL LAW

The development of the multirate proportional-plus-integral control law is presented here. An overview of the multirate PI structures and the key steps in designing these controllers is given in Section 3.2.1. The mathematical basis for the multirate PI development is comprised of the continuous-time and single-rate digital version of the PI controller which are described in Section 3.2.2; the extension to the multirate case is outlined in Section 3.2.3.

3.2.1 Multirate Proportional-Plus-Integral Control Structures

Two alternative methods of holding slow controls in a multirate PI control structure are shown in Figs. 3.2-1 and 3.2-2. The structure in Fig. 3.2-1 uses the forward path integration function to hold slow controls; augmentation of the

R-49709a

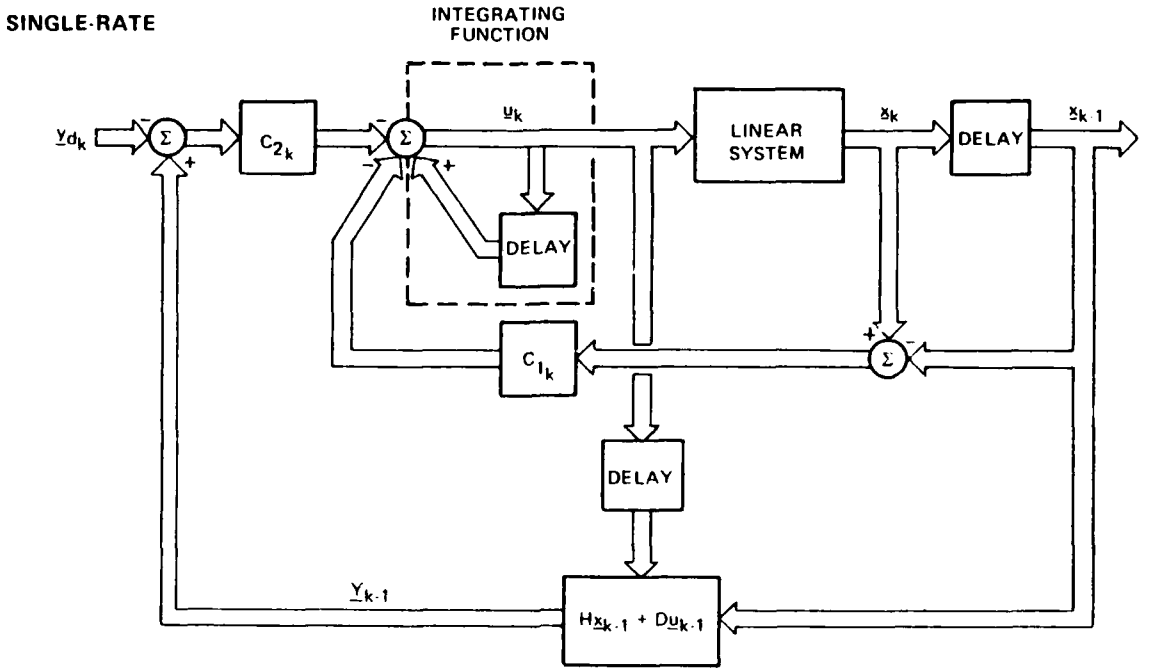

Figure 3.2-1 Multirate PI Structure Using Integrators as Holding Circuits

R-49712b

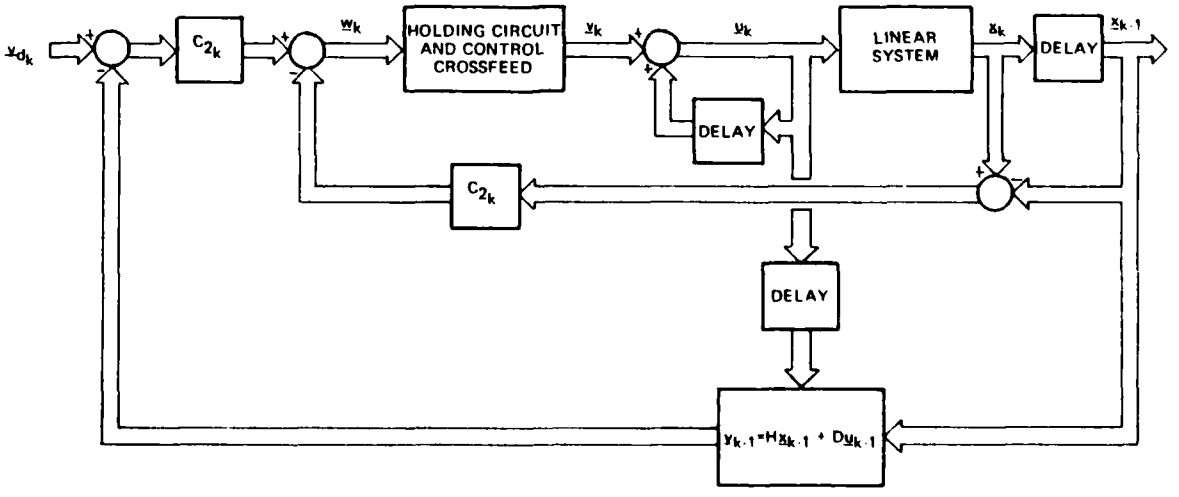

Figure 3.2-2 Multirate PI Structure Using Explicit Holding Circuit States

system dynamics with slow control holding circuits is used in Fig. 3.2-2. The structure of Fig. 3.2-2 is used when smooth transitions of the slow controls between new computations are desired; the effect of the slow control holding circuit on a typical control history is shown in Fig. 3.2-3. On a slow control computation cycle the structure of Fig. 3.2-1 computes a new integrator input which results in a step change of the slow control. The structure of Fig. 3.2-2 computes a new "staircase" increment which is added to the control on each succeeding fast computational cycle by the integrator dynamics; hence, the holding circuit structure provides for smoother transitions of the slow controls between new control computations and, therefore, a smoother plant response.

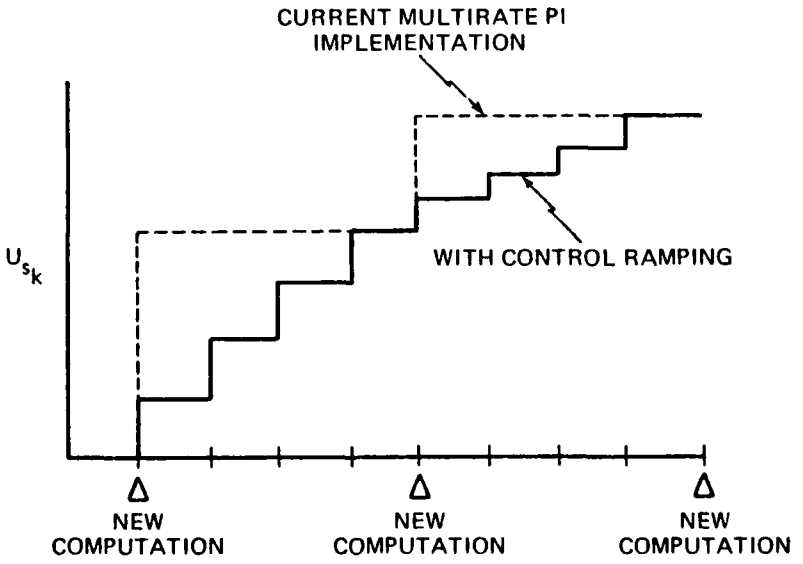

Figure 3.2-3 Typical Slow Control Histories for the Two PI Structures

Extension of the PI control formulation (which is discussed in detail in Section 3.3) to the multirate case is accomplished by a procedure similar to that used to formulate the multirate regulator:

- A construct is introduced into the discrete-time plant dynamics to hold controls computed at low sample rates.
- The resulting discrete-time dynamics are used with the relationships presented in Ref. 5 to derive multirate cost functional weighting matrices.
- The multirate dynamics and cost functional weighting matrices are substituted into the discrete-time Ricatti equation. Regulator gains are derived from the periodic steady-state solution of the Ricatti equation.
- The pure integration function in the forward path of the control structure is recovered by a transformation of the feedback variables.

The first three steps are directly analogous to the multirate regulator design procedure; i.e., incorporation of a slow control holding function into the plant dynamics, computation of weighting matrices, and solution of a periodic Ricatti equation for the gains. The last step is required to obtain the desired integrating function in the forward path of the control structure; this transformation is described in the mathematical development of Sections 3.2.2 and 3.2.3.

3.2.2 Continuous-Time and Single-Rate Digital PI Control

Continuous-Time PI Controller - The mathematical development of the continuous-time PI control structure is

initiated by augmenting the plant state vector, $\underline{x}$, with the plant controls, $\underline{u}$, and introduction of control rate inputs, $\underline{v}$, to drive the augmented system, i.e.,:

$$\begin{bmatrix} \dot{\underline{x}} \\ \hline \dot{\underline{u}} \end{bmatrix} = \begin{bmatrix} F & G \\ \hline 0 & 0 \end{bmatrix} \begin{bmatrix} \underline{x} \\ \hline \underline{u} \end{bmatrix} + \begin{bmatrix} 0 \\ \hline I \end{bmatrix} \underline{v} \qquad (3.2\text{-}1)$$

The output, $\underline{y}$, of this augmented system is given by:

$$\underline{y} = H\underline{x} + D\underline{u} \qquad (3.2\text{-}2)$$

The continuous-time cost functional (with an infinite time-horizon) to be minimized by control is given by:

$$J = \frac{1}{2} \int_0^\infty \left\{ (\Delta\underline{x}^T \; \Delta\underline{u}^T) Q \begin{bmatrix} \Delta\underline{x} \\ \hline \Delta u \end{bmatrix} + \underline{v}^T R \underline{v} \right\} dt \qquad (3.2\text{-}3)$$

Here $\Delta\underline{x}$ and $\Delta\underline{u}$ are state and control errors relative to a non-zero set point, $(\underline{x}^*, \underline{u}^*)$, i.e.,

$$\Delta\underline{x} = \underline{x} - \underline{x}^* \quad ; \quad \Delta\underline{u} = \underline{u} - \underline{u}^* \qquad (3.2\text{-}4)$$

For zero steady-state output error to a step input (i.e., a constant, non-zero set point)

$$\underline{y}_d = H\underline{x}^* + D\underline{u}^* \qquad (3.2\text{-}5)$$

also in steady state:

$$\dot{\underline{x}} = \underline{0} = F\underline{x}^* + G\underline{u}^* \qquad (3.2\text{-}6)$$

Combining Eqs. 3.2-4 and 3.2-5:

$$\begin{bmatrix} 0 \\ --- \\ \underline{y}_d \end{bmatrix} = \begin{bmatrix} F & G \\ & \\ H & D \end{bmatrix} \begin{bmatrix} \underline{x}^* \\ --- \\ \underline{u}^* \end{bmatrix} \tag{3.2-7}$$

For the case of $\underline{y}_d$ and $\underline{u}$ of equal dimension, the vectors $\underline{x}^*$ and $\underline{u}^*$ will exist and be unique for arbitrary choice of $\underline{y}_d$ if the composite matrix has an inverse:

$$\begin{bmatrix} F & G \\ H & D \end{bmatrix}^{-1} = \begin{bmatrix} S_{11} & S_{12} \\ S_{21} & S_{22} \end{bmatrix} \tag{3.2-8}$$

Hence,

$$\underline{x}^* = S_{12}\underline{y}_d \quad ; \quad \underline{u}^* = S_{22}\underline{y}_d \tag{3.2-9}$$

Noting that the dynamics of $\Delta\underline{x}$ and $\Delta\underline{u}$ are also given by Eq. 3.2-1 (for constant $\underline{x}^*$ and $\underline{u}^*$), regulator gains for the augmented system can be derived by solving the time-invariant form of the continuous Ricatti equation:

$$0 = P\hat{F} + \hat{F}^T P + Q - P\hat{G}R^{-1}\hat{G}^T P \tag{3.2-10}$$

$$C^T = -R^{-1}\hat{G}^T P \tag{3.2-11}$$

with

$$\hat{F} = \begin{bmatrix} F & G \\ 0 & 0 \end{bmatrix} \tag{3.2-12}$$

$$\hat{G} = \begin{bmatrix} 0 \\ I \end{bmatrix} \tag{3.2-13}$$

The control structure that results from the gain, C, is shown in Fig. 3.2-4. Note that the controller requires knowledge of $\underline{x}^*$ and $\underline{u}^*$, and that the control Δu is low-pass filtered than having a pure integration in the forward control path.

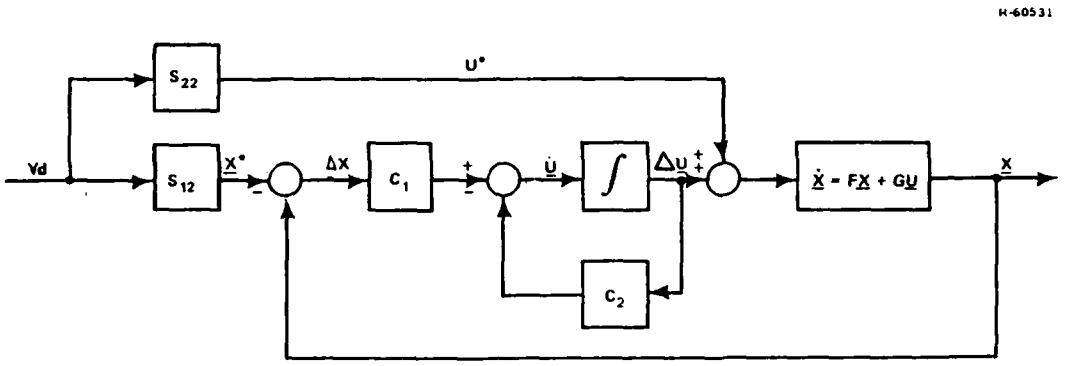

Figure 3.2-4 Tracking Control Structure

The control structure of Fig. 3.2-2 can be converted into the desired proportional-plus-integral structure by using Eq. 3.2-6 to transform the feedback variables from $\Delta\underline{x}$ and $\Delta\underline{u}$ to $\Delta\underline{x}$ and $(\underline{y}_d-\underline{y})$, i.e.,:

$$\begin{bmatrix} \dot{\underline{x}} \\ \hline (\underline{y}_d-\underline{y}) \end{bmatrix} = \begin{bmatrix} F & G \\ H & D \end{bmatrix} \begin{bmatrix} (\underline{x}^*-\underline{x}) \\ \hline (\underline{u}^*-\underline{u}) \end{bmatrix} \tag{3.2-14}$$

$$\begin{bmatrix} (\underline{x}^*-\underline{x}) \\ (\underline{u}^*-\underline{u}) \end{bmatrix} = \begin{bmatrix} S_{11} & S_{12} \\ S_{21} & S_{22} \end{bmatrix} \begin{bmatrix} \dot{\underline{x}} \\ (\underline{y}_d-\underline{y}) \end{bmatrix} \tag{3.2-15}$$

The control law is thus transformed:

$$\underline{v} = \dot{\underline{u}} = C_1(\underline{x}^* - \underline{x}) + C_2(\underline{u}^* - \underline{u}) \tag{3.2-16}$$

$$= C_1[S_{11}\dot{\underline{x}} + S_{12}(\underline{y}_d - \underline{y})] + C_2[S_{21}\dot{\underline{x}} + S_{22}(\underline{y}_d - \underline{y})] \tag{3.2-17}$$

$$= \underbrace{(C_1S_{11} + C_2S_{21})}_{C_1'}\dot{\underline{x}} + \underbrace{(C_1S_{12} + C_2S_{22})}_{C_2'}(\underline{y}_d - \underline{y}) \tag{3.2-18}$$

Integrating:

$$(\underline{u} - \underline{u}_o) = C_1'(\underline{x} - \underline{x}_o) + C_2' \int_{t_o}^{t} (\underline{y}_d - \underline{y})dt \tag{3.2-19}$$

The structure of the closed-loop system described by Eq. 3.2-19 is shown in Fig. 3.2-5; the controller has the pure integrating function which ensures that the output error, $(\underline{y}_d - \underline{y})$ will be driven to zero in steady-state.

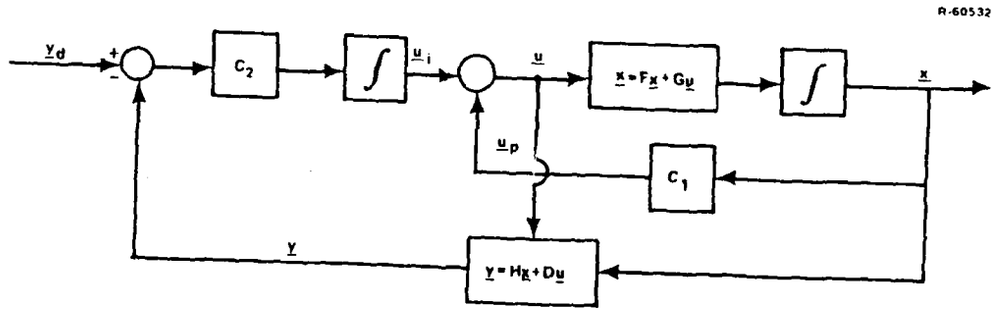

Figure 3.2-5 Proportional-Plus-Integral Control Structure

Single-Rate Digital PI Controller - The single-rate digital PI controller can be derived from the continuous-time PI controller in the same manner that the single-rate regulator

was derived from the continuous-time regulator in Section 2.3. Again, the discrete-time representation of the augmented system dynamics (Eq. 3.2-1) is used along with the weighting matrix relationships of Ref. 5 to transform the continuous-time problem into the discrete-time domain. The transformation procedure is summarized in Table 3.2-1.

Once the discrete-time representation of dynamics and the cost functional weighting matrices have been derived, regulator gains are obtained by solution of the steady-state form of the discrete Ricatti equation. Again, the control structure resulting from the derived gains lacks the desired pure integration function; a transformation of the feedback variables to obtain a pure integration of the output error, $(\underline{y}_d - \underline{y}_k)$, is required. The solution of the optimal control problem and the feedback transformation are summarized in Table 3.2-2.

The structure of the closed-loop discrete-time PI controller is shown in Fig. 3.2-6. Again, the indicated integrating function in the forward path ensures that the steady-state error to constant $\underline{y}_d$ is driven to zero.

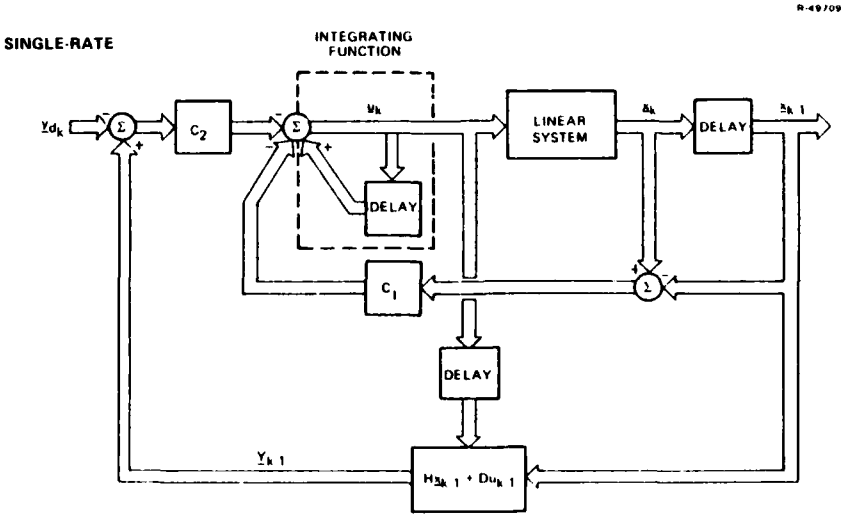

Figure 3.2-6 Discrete-Time Proportional-Plus-Integral Controller

TABLE 3.2-1

TRANSFORMATION OF THE CONTINUOUS-TIME OPTIMAL CONTROL PROBLEM TO DISCRETE-TIME

T-2901

CONTINUOUS-TIME AIRCRAFT MODEL ERROR DYNAMICS WITH COMPENSATOR

$$\begin{bmatrix} \Delta\dot{\underline{x}} \\ \Delta\dot{\underline{u}} \end{bmatrix} = \begin{bmatrix} F & G \\ 0 & 0 \end{bmatrix} \begin{bmatrix} \Delta\underline{x} \\ \Delta\underline{u} \end{bmatrix} + \begin{bmatrix} 0 \\ I \end{bmatrix} \Delta\underline{v}$$

CONTINUOUS-TIME COST FUNCTION

$$J = \int_0^\infty \left\{ [\Delta\underline{x}^T \ \Delta\underline{u}^T] \, Q \begin{bmatrix} \Delta\underline{x} \\ \Delta\underline{u} \end{bmatrix} + [\Delta\underline{v}^T R \Delta\underline{v}] \right\} dt$$

DISCRETE-TIME MODEL

$$\Phi = e^{F\Gamma_s} \qquad \Gamma = \int_0^{T_s} e^{F\tau} \, d\tau \, G$$

$$\begin{bmatrix} \Delta\underline{x} \\ \Delta\underline{u} \end{bmatrix}_{k+1} = \begin{bmatrix} \Phi & \Gamma \\ 0 & I \end{bmatrix} \begin{bmatrix} \Delta\underline{x} \\ \Delta\underline{u} \end{bmatrix}_k + \begin{bmatrix} 0(T_s^2) \\ T_s I \end{bmatrix} \Delta\underline{v}_k$$

DISCRETE-TIME COST FUNCTION

$$J = \sum_{k=-1}^{\infty} [\Delta\underline{x}^T \ \Delta\underline{u}^T \ \Delta\underline{v}^T]_k \begin{bmatrix} \overline{Q} & \overline{M} \\ \overline{M}^T & \overline{R} \end{bmatrix} \begin{bmatrix} \Delta\underline{x} \\ \Delta\underline{u} \\ \Delta\underline{v} \end{bmatrix}_k$$

DISCRETE-TIME WEIGHTING MATRICES

$$Q = \int_0^{T_s} e^{\begin{bmatrix} F & G \\ 0 & 0 \end{bmatrix}^T t} \, Q \, e^{\begin{bmatrix} F & G \\ 0 & 0 \end{bmatrix} t} \, dt$$

$$M = \int_0^{T_s} e^{\begin{bmatrix} F & G \\ 0 & 0 \end{bmatrix}^T t} \, Q \left[\int_0^t e^{\begin{bmatrix} F & G \\ 0 & 0 \end{bmatrix} s} \, ds \right] dt \begin{bmatrix} 0 \\ I \end{bmatrix}$$

$$R = T_s R + [0 \ I] \int_0^{T_s} \left[\int_0^t e^{\begin{bmatrix} F & G \\ 0 & 0 \end{bmatrix}^T s} \, ds \right] Q \left[\int_0^t e^{\begin{bmatrix} F & G \\ 0 & 0 \end{bmatrix} \tau} \, d\tau \right] dt \begin{bmatrix} 0 \\ I \end{bmatrix}$$

TABLE 3.2-2

SOLUTION OF THE DISCRETE-TIME OPTIMAL CONTROL PROBLEM

T-4350

DISCRETE-TIME RICATTI EQUATION

$$L_k = (\hat{\Gamma}^T P_{k+1} \hat{\Gamma} + \overline{R})^{-1} \hat{\Gamma}^T P_{k+1}$$

$$P_k = \theta^T (I - L_k \hat{\Gamma}^T) P_{k+1} \theta + Q^*$$

where $\theta \equiv \hat{\Phi} - \hat{\Gamma} \overline{R}^{-1} \overline{M}^T$

$$\overline{Q}^* \equiv \overline{Q} - \overline{M} \overline{R}^{-1} \overline{M}^T$$

$$\hat{\Phi} = \left[\begin{array}{c|c} \Phi & \Gamma \\ \hline 0 & I \end{array}\right]$$

$$\hat{\Gamma} = \begin{bmatrix} 0(T_s^2) \\ \hline T_s I \end{bmatrix}$$

REGULATOR GAINS

$$[C_1 C_2] = \overline{R}^{-1} \overline{M}^T + L\theta$$

PROPORTIONAL-PLUS-INTEGRAL CONTROL LAW GAINS

$$[C_1' \quad T_s C_2'] = T_s [C_1 C_2] \begin{bmatrix} (\Phi - I) & \Gamma \\ H & D \end{bmatrix}^{-1}$$

PROPORTIONAL-PLUS-INTEGRAL CONTROL LAW

$$\underline{u}_k = \underline{u}_{k-1} - C_1'(\underline{x}_k - \underline{x}_{k-1}) + T_s C_2'(\underline{y}_d - y_{k-1})$$

3.2.3 Multirate Digital PI Control

The extension of the PI control formulation to the multirate case is outlined in this section. The two alternative PI structures described in Section 3.2.1 are considered. Again, the mathematical procedure for deriving multirate PI controllers is very similar to that used to derive the multirate regulator.

Multirate PI Controller Using Integrator Hold - Formulation of the multirate PI controller using the integrators to hold slow controls follows from a simple modification of the augmented plant dynamics to accommodate control sequencing. This modification is described by Eqs. 3.2-20 and 3.2-21.

$$\begin{bmatrix} \underline{x}_{k+1} \\ \underline{u}_{k+1} \end{bmatrix} = \left[\begin{array}{c|c} \Phi & \Gamma \\ \hline 0 & I \end{array}\right] \begin{bmatrix} \underline{x}_k \\ \underline{u}_k \end{bmatrix} + \begin{bmatrix} 0 \\ T_s \Delta_k \end{bmatrix} \underline{v}_k \tag{3.2-20}$$

$$\Delta_k = \begin{bmatrix} \delta_{k,i_1\ell_1} & 0 & \cdots & 0 \\ 0 & \delta_{k,i_2\ell_2} & & \vdots \\ \vdots & & 0 & \vdots \\ 0 & \cdots & 0 & \delta_{k,i_m\ell_m} \end{bmatrix} \tag{3.2-21}$$

with:

$$\delta_{k,i_j\ell_j} = \begin{cases} 1; i_j\ell_j = k \\ 0; i_j\ell_j \neq k \end{cases} \tag{3.2-22}$$

The matrix, Δ_k, schedules the inputs to the control integrators. For example, if u_2 is updated every two cycles

(i.e., ℓ_2=2) the element of Δ_k that controls the incrementation of u_2 will be zero on cycles when k is not a multiple of 2 (i.e., when $k \neq i_2 \ell_2$).

The multirate PI cost functional is given by:

$$J = \frac{1}{2} \sum_{k=0}^{\infty} \left\{ (\underline{x}_k^T \; \underline{u}_k^T) \; \hat{Q}_k \begin{pmatrix} \underline{x}_k \\ \hline \underline{u}_k \end{pmatrix} + 2(\underline{x}_k^T \; \underline{u}_k^T) \; \hat{M}_k \underline{v}_k + \underline{v}_k^T \hat{R}_k \underline{v}_k \right\} \tag{3.2-23}$$

The matrices $\hat{Q}_k$, $\hat{M}_k$, $\hat{R}_k$ are derived by substituting the dynamic model given by Eq. 3.2-20 into the relationships from Ref. 5.

$$\hat{Q}_k = \int_0^{T_s} \hat{\Phi}^T(t,0) Q \; \hat{\Phi}(t,0) dt \tag{3.2-24}$$

$$\hat{M}_k = \int_0^{T_s} \hat{\Phi}^T(t,0) Q \begin{bmatrix} 0 \\ \hline T_s \Delta_k \end{bmatrix} dt \tag{3.2-25}$$

$$\hat{R}_k = T_s R + \int_0^{T_s} [0 \quad T_s \Delta_k^T] \; Q \begin{bmatrix} 0 \\ \hline T_s \Delta_k \end{bmatrix} dt \tag{3.2-26}$$

Where Q and R are the cost functional matrices corresponding to a continuous-time PI controller having desired dynamics. Equations 3.2-25 and 3.2-26 can be rearranged:

$$\hat{M}_k = \int_0^{T_s} \hat{\Phi}^T(t,0) Q \begin{bmatrix} 0 \\ \hline T_s I \end{bmatrix} dt \; \Delta_k \tag{3.2-27}$$

$$\hat{R}_k = T_s R + \Delta_k^T \int_0^{T_s} [0 \quad T_s I] \, Q \begin{bmatrix} 0 \\ --- \\ T_s I \end{bmatrix} dt \, \Delta_k \qquad (3.2\text{-}28)$$

As Eq. 3.2-27 and 3.2-28 indicate, the multirate PI cost functional matrices can be derived from their single rate counterparts by multiplying by Δ_k where appropriate.

Given the system dynamics, Eq. 3.2-20, and the set of $\hat{Q}_k$, $\hat{M}_k$, and $\hat{R}_k$ matrices over a complete control cycle, regulator gains can be derived by determining the periodic steady-state solution of the discrete-time Riccatti equation, i.e., propagate:

$$L_k = (\hat{\Gamma}^T P_{k+1} \hat{\Gamma} + \bar{R})^{-1} \hat{\Gamma}^T P_{k+1} \qquad (3.2\text{-}29)$$

$$P_k = \theta_k^T (I - L_k^T \hat{\Gamma}^T) P_{k+1} \theta_k + Q_k^* \qquad (3.2\text{-}30)$$

where

$$\theta_k = \hat{\Phi} - \hat{\Gamma}_k \hat{R}_k^{-1} \hat{M}_k^T \qquad (3.2\text{-}31)$$

$$Q_k^* = \hat{Q}_k - \hat{M}_k \hat{R}_k^{-1} \hat{M}_k^T \qquad (3.2\text{-}32)$$

and the control gains in steady-state are given by:

$$[C_1 \quad C_2]_k = \hat{R}_k^{-1} \hat{M}_k^T + L_k \theta_k \; ; \quad k=1,2,\ldots \ell \qquad (3.2\text{-}33)$$

Again, the pure integration function in the forward path is recovered through transformation of the feedback variables:

$$[C_1' \; T_s C_2']_k = T_s \Delta_k [C_1 \; C_2]_k \begin{bmatrix} (\Phi - I) & \Gamma \\ H & D \end{bmatrix}^{-1} \; ; \; k=1,2,\ldots \ell \qquad (3.2\text{-}34)$$

The presence of Δ_k in Eq. 3.2-34 will zero low-rate control gains on cycles between computations of the low-rate controls. The control implementation of the multirate PI controller is given by:

$$\underline{u}_k = \underline{u}_{k-1} - C_{1k}(\underline{x}_k - \underline{x}_{k-1}) + T_s C_{2k}(\underline{y}_d - \underline{y}_{k-1}) \qquad (3.2\text{-}35)$$

This control algorithm is represented by the structure of Fig. 3.2-5.

Multirate PI Controller Using Explicit Holding Circuit Augmentation

If explicit holding circuit states are introduced to hold low rate controls between updates, the PI formulation follows a development very similar to that of the basic multirate regulator; i.e.,:

- The plant dynamics are augmented with holding circuit states
- Multirate cost functional matrices are constructed from partitions of the corresponding single-rate matrices
- Regulator gains are derived from the periodic steady-state solution of the discrete-time Ricatti equation
- The pure integration function in the forward path is recovered by transformation of the feedback variables.

The first three steps in the design process are identical to those for the multirate regulator and, therefore, will only be summarized here.

The discrete-time dynamics augmented by holding circuit states are given by:

$$\begin{bmatrix} \underline{x} \\ \underline{u}_f \\ \underline{u}_s \\ \underline{v}_s \end{bmatrix}_{k+1} = \begin{bmatrix} \Phi & \Gamma_f & \Gamma_s & 0 \\ 0 & I & 0 & 0 \\ 0 & 0 & I & IT_s \\ 0 & 0 & 0 & I \end{bmatrix} \begin{bmatrix} \underline{x} \\ \underline{u}_f \\ \underline{u}_s \\ \underline{v}_s \end{bmatrix}_k + \begin{bmatrix} 0 & 0 \\ IT_s & 0 \\ 0 & IT_s\Delta_k \\ 0 & I\Delta_k \end{bmatrix} \begin{bmatrix} \underline{v}_f \\ \underline{w}_s \end{bmatrix}_k \tag{3.2-36}$$

$$\tilde{\underline{x}}_{k+1} = \tilde{\Phi}\tilde{\underline{x}}_k + \tilde{\Gamma}_k\tilde{\underline{u}}_k \tag{3.2-37}$$

Again, Δ_k nulls the input to the holding circuits of low rate control increments, $\underline{v}_s$, on cycles between new computations of those increments.

Using the dynamics given by Eq. 3.2-36 and the relationships presented in Ref. 5, the multirate cost functional matrices are given by:

$$\tilde{Q}_k = \left[\begin{array}{c|c} \overline{Q} & \overline{M}_s \\ \hline \overline{M}_s^T & \overline{R}_s \end{array}\right] \tag{3.2-38}$$

$$\tilde{M}_k = \left[\begin{array}{c|c} \overline{M}_f & \overline{R}_{fs}\Delta_k \\ \hline \overline{R}_{fs}^T & \overline{R}_s\Delta_k \end{array}\right] \tag{3.2-39}$$

$$\tilde{R}_k = \left[\begin{array}{c|c} \overline{R}_f & \overline{R}_{fs}\Delta_k \\ \hline \Delta_k^T\overline{R}_{fs} & \Delta_k^T\overline{R}_s\Delta_k \end{array}\right] \tag{3.2-40}$$

As in the regulator case (Section 2.3) the multirate cost functional matrices can be constructed from appropriate

partitions of the single rate cost functional matrices (i.e., partitions corresponding to the base rate and low rate controls); Δ_k selects those rows and columns of the partitions to be retained in the cost functional matrices on a particular cycle.

Regulator gains are derived again from the steady-state solution of the discrete-time Ricatti equation:

$$L_k = (\tilde{\Gamma}_k^T P_{k+1} \tilde{\Gamma}_k + \tilde{R})^{-1} \tilde{\Gamma}^T P_{k+1} \tag{3.2-41}$$

$$P_k = \tilde{\theta}_k^T (I - L_k^T \tilde{\Gamma}_k^T) P_{k+1} \tilde{\theta}_k + Q_k^* \tag{3.2-42}$$

$$\tilde{\theta}_k = \tilde{\Phi} - \tilde{\Gamma}_k \tilde{R}_k^{-1} \tilde{M}_k^T \tag{3.2-43}$$

$$Q_k^* = \tilde{Q}_k - \tilde{M}_k \tilde{R}_k^{-1} \tilde{M}_k^T \tag{3.2-44}$$

and the gains are given by:

$$(C_1 \; C_2 \; C_3) = \tilde{R}_k^{-1} \tilde{M}_k^T + L_k \tilde{\theta}_k \; ; \; k=1,2,\ldots \ell \tag{3.2-45}$$

where C_1, C_2, and C_3 multiply the plant state ($\underline{x}$), control ($\underline{u}$), and slow control increment ($\underline{v}_s$), respectively. The pure integration function in the forward path is recovered by transforming the feedback variables:

$$[C_1' \; T_s C_2' \; T_s C_3']_k = T_s [C_1 \; C_2 \; C_3]_k \left[\begin{array}{cc:c} (\Phi - I) & \Gamma & \\ H & D & 0 \\ \hdashline & 0 & I \end{array}\right]^{-1} \tag{3.2-46}$$

The control implementation is given by:

$$\underline{u}_k = \underline{u}_{k-1} - C_{1k}'(\underline{x}_k - \underline{x}_{k-1}) + T_s C_{2k}'(\underline{y}_d - \underline{y}_{k-1}) + T_s C_{3k}'\underline{v}_{s_k} \tag{3.2-47}$$

3.3 EXAMPLE MULTIRATE PI SYSTEM

The properties and performance of a multirate proportional-plus-integral flight control system are described in this section. The plant used in this example is the linearized dynamics of the F-14 aircraft in trimmed level flight.

3.3.1 Plant Description

The plant to be controlled is the linearized dynamics of the F-14 in trimmed level flight at an altitude of 20,000 ft with a velocity of 183 m/sec (600 ft/sec). A discrete-time representation based on a sample rate of 20 Hz is used:

$$\underline{x}_{k+1} = \Phi \underline{x}_k + \Gamma \underline{u}_k \tag{3.3-1}$$

$$\underline{x}_k^T = (q_b, w, v, r_b, p_b)_k \tag{3.3-2}$$

= (vertical velocity, pitch rate, sideslip velocity, yaw rate, roll rate)

$$\underline{u}_k^T = (\delta_s, \delta_{mf}, \delta_{sp}, \delta_{ds}, \delta_r) \tag{3.3-3}$$

= (stabilator, maneuver flap, spoiler, differential stabilator, rudder)

The values of the Φ and Γ matrices used in this example are presented in Ref. 10.

The control system will use direct measurement feedback (assuming appropriate instrument prefiltering) of the three body rotation rates -- q_b, r_b, p_b -- and of the normal and lateral acceleration. Sideslip and normal velocity measurements will be available at the 20-Hz base rate.

The command set (i.e., the desired system output) is described by:

$$\underline{y}_{d_k} = H\underline{x}_k + D\underline{u}_k \qquad (3.3\text{-}4)$$

$$\underline{y}_{d_k}^T = (a_n, \delta_{mf}, p_s, a_y, \delta_{sp}) \qquad (3.3\text{-}5)$$

= (normal acceleration, maneuver flap, stability-axis roll rate, lateral acceleration, spoiler)

Inclusion of δ_{mf} and δ_{sp} implies that maneuver flap and spoiler are commanded to nominal settings by the pilot (i.e., the pilot does not actively command these surfaces) but are free to be activated by the control system during transients.

3.3.2 Control System Design

The goal of the control system design is to synthesize a multirate PI controller equivalent to that described in Ref. 10. To this end, the state, control, and control rate weighting matrices used to develop the multirate design are identical to those used in Ref. 10.

The multirate PI control system structure uses the integrator states to hold slow controls between updates. The vehicle dynamics augmented by the control integrators are given by:

$$\begin{bmatrix} \underline{x}_{k+1} \\ \underline{u}_{k+1} \end{bmatrix} = \left[\begin{array}{c|c} \phi & \Gamma \\ \hline 0 & I \end{array}\right] \begin{bmatrix} \underline{x}_k \\ \underline{u}_k \end{bmatrix} + \begin{bmatrix} 0 \\ T_s \Delta_k \end{bmatrix} \underline{v}_k \qquad (3.3\text{-}6)$$

The sequence of operation for the five control surfaces is defined in Table 3.3-1. Each row of Table 3.3-1 defines the value of the diagonal element of Δ_k for each control surface. As the table entries show, the control computations are scheduled so that on any given cycle three controls are computed; based on ten multiplications per control calculation (neglecting addition times), the schedule in Table 3.3-1 represents a 40 percent reduction in computational load over a single-rate (20-Hz) implementation.

Using the dynamics described by Eq. 3.3-6 and the multirate weighting matrices defined by Eqs. 3.2-24, 3.2-27 and 3.2-28, Eqs. 3.2-29 and 3.2-30 are propagated to periodic steady-state. The periodic regulator gains are computed by Eq. 3.2-33 and are transformed into the PI structure by Eq. 3.2-34.

TABLE 3.3-1
MULTIRATE PI CONTROL SCHEDULE

DISCRETE-TIME INDEX, k	δ_s	δ_{mf}	δ_{sp}	δ_{ds}	δ_r
$i\ell+1$	0	1	1	1	0
$i\ell+2$	1	0	0	1	1
$i\ell+3$	1	1	0	1	0
$i\ell+4$	1	0	0	1	1

Figure 3.3-1 shows the values of the periodic stabilator gains along with the equivalent single-rate gains. The

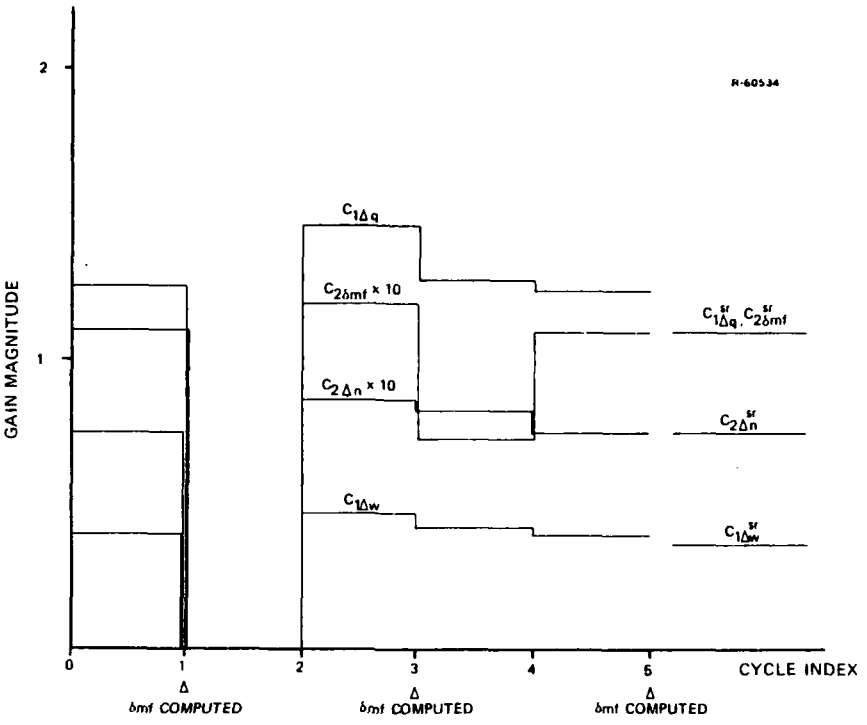

Figure 3.3-1 Stabilator Gains

pitch rate and vertical velocity proportional gains (C_{1_q} and C_{1_w}) vary significantly over the four cycle period; this variation is a result of skipping the stabilator computation on Cycle 1. The integral feedback gains, $C_{2_{\delta mf}}$ and $C_{2_{an}}$, also show variations over the control period. The effect of maneuver flap computations on $C_{2_{\delta mf}}$ is evident from Fig. 3.3-1; $C_{2_{\delta mf}}$ is reduced significantly on Cycle 3 when a new value of δ_{mf} is computed. On cycles between δ_{mf} computations, δ_{mf} is crossfed to the stabilator; this crossfeed is reduced on cycles when a new δ_{mf} is computed.

Figure 3.3-2 shows the values of the differential stabilator gains along with their corresponding single-rate

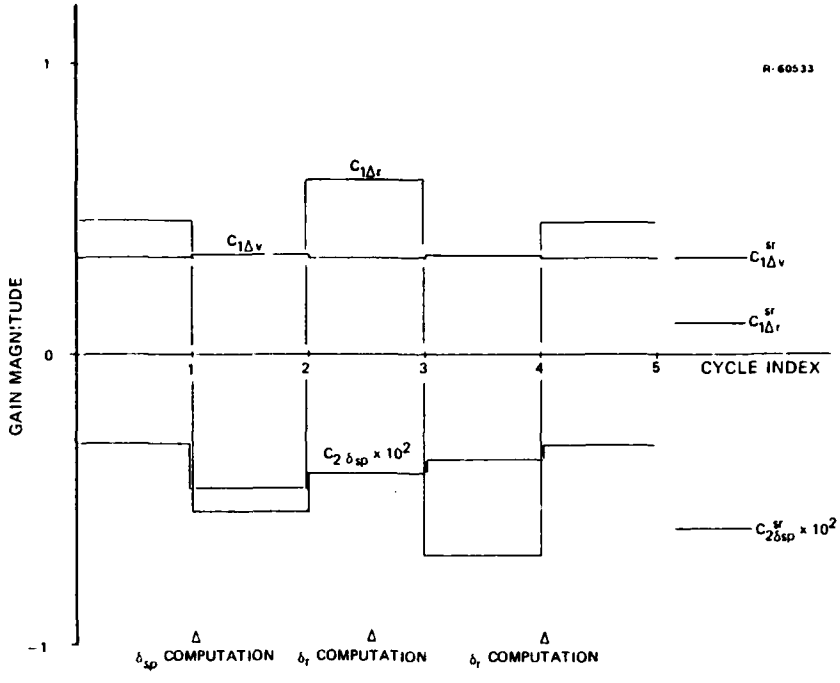

Figure 3.3-2 Differential Stabilator Gains

values. The roll rate to differential stabilator gain is not plotted; its value is constant over the control cycle and equal to the single-rate value. As in the regulator example (Section 2.5.3), the roll control channel is the natural inner loop of this system; it should be expected that the single rate and multirate gain should be similar. The other feedback gains do show considerable variations, particularly the yaw rate to differential stabilator gain, C_{l_r}. The latter changes sign every cycle; again, the gain variations are a result of the controller using differential stabilator to compensate the Dutch Roll mode on cycles between rudder updates.

3.3.3 System Properties

The evaluation of the multirate PI controller presented here includes:

- Comparison of the closed-loop eigenvalues of the multirate PI controller with those of the equivalent single-rate PI controller (i.e., the single-rate controller designed from the equivalent weighting matrices.)
- Comparison of the multirate PI system transient response with that of the equivalent single rate system.

Evaluation of the error rejection properties of the multirate PI controller is covered in a broad context in Chapter 4.

Eigenvalues of the PI Controllers - The closed-loop eigenvalues of the multirate PI system and the equivalent single-rate PI system are listed in Table 3.3-2. These eigenvalues are the mapped continuous-time eigenvalues generated by the method of Section 2.4. Some relatively small variations of eigenvalues exist between the two controllers for the vehicle motion modes (i.e., short period, roll command, dutch roll, normal acceleration command, and sideslip command modes) and some relatively large variations in the longitudinal control (i.e., maneuver flap) and lateral control (i.e., rudder/spoiler) modes. The small variations result from an approximation in the augmented system control effectiveness matrix used to derive the weighting matrices for the two control designs.

Recall that the discrete-time description of the augmented system dynamics are given by:

TABLE 3.3-2

COMPARISON OF MAPPED CLOSED-LOOP EIGENVALUES

DYNAMIC MODE	SINGLE RATE PI			MULTIRATE PI		
	NATURAL FREQUENCY, rad/sec	DAMPING RATIO	TIME CONSTANT, sec	NATURAL FREQUENCY, rad/sec	DAMPING RATIO	TIME CONSTANT, sec
Short Period	5.20	0.889	-	4.93	0.770	-
Roll Command	4.32	0.675	-	4.29	0.700	-
Dutch Roll	3.54	0.714	-	3.04	0.642	-
Normal Acceleration Command	-	-	0.275	-	-	0.313
Longitudinal Control	-	-	0.798	-	-	1.25
Lateral Control	-	-	1.64	-	-	3.22
Sideslip Command	-	-	1.19	-	-	1.24

$$\begin{bmatrix} \underline{x} \\ \underline{u} \end{bmatrix}_{k+1} = \begin{bmatrix} \Phi & \Gamma \\ 0 & I \end{bmatrix} \begin{bmatrix} \underline{x} \\ \underline{u} \end{bmatrix}_k + \begin{bmatrix} O(T_s^2) \\ T_s I \end{bmatrix} v_k \qquad (3.3\text{-}7)$$

The $O(T_s^2)$ term is neglected in order that the augmented system dynamics represent the plant dynamics coupled to the controls, $\underline{u}$, by zero order holds; inclusion of the $O(T_s^2)$ term represents a first-order hold implementation.

Although neglect of the $O(T_s^2)$ term is a slight approximation, the direct correspondence of the continuous-time and single-rate digital control designs (i.e., digital weighting matrices computed from specified continuous-time weighting matrices) is lost. The effect of the approximation is enhanced in the multirate case since the optimization problem is formulated over an ℓ-cycle control period (in this case over four cycles); hence, variations of the vehicle mode eigenvalues exist between the single-rate and multirate systems. The significant eigenvalue variations of the longitudinal and lateral control modes reflects a difference in the optimization problem solutions for the single-rate and multirate controllers. If the maneuver flap and rudder are run at a lower rate, the optimization problem selects a lower bandwidth (i.e., a larger time-constant) for their respective low-pass filter functions (recall the control structure of Fig. 3.2-2 and the fact that transforming to the PI structure does not alter the system eigenvalues).

Although variations in the eigenvalues exist, the transient responses of the two closed-loop systems are very similar. These responses are compared next.

System Transient Responses - The primary longitudinal control response, normal acceleration, is shown in Fig. 3.3-3

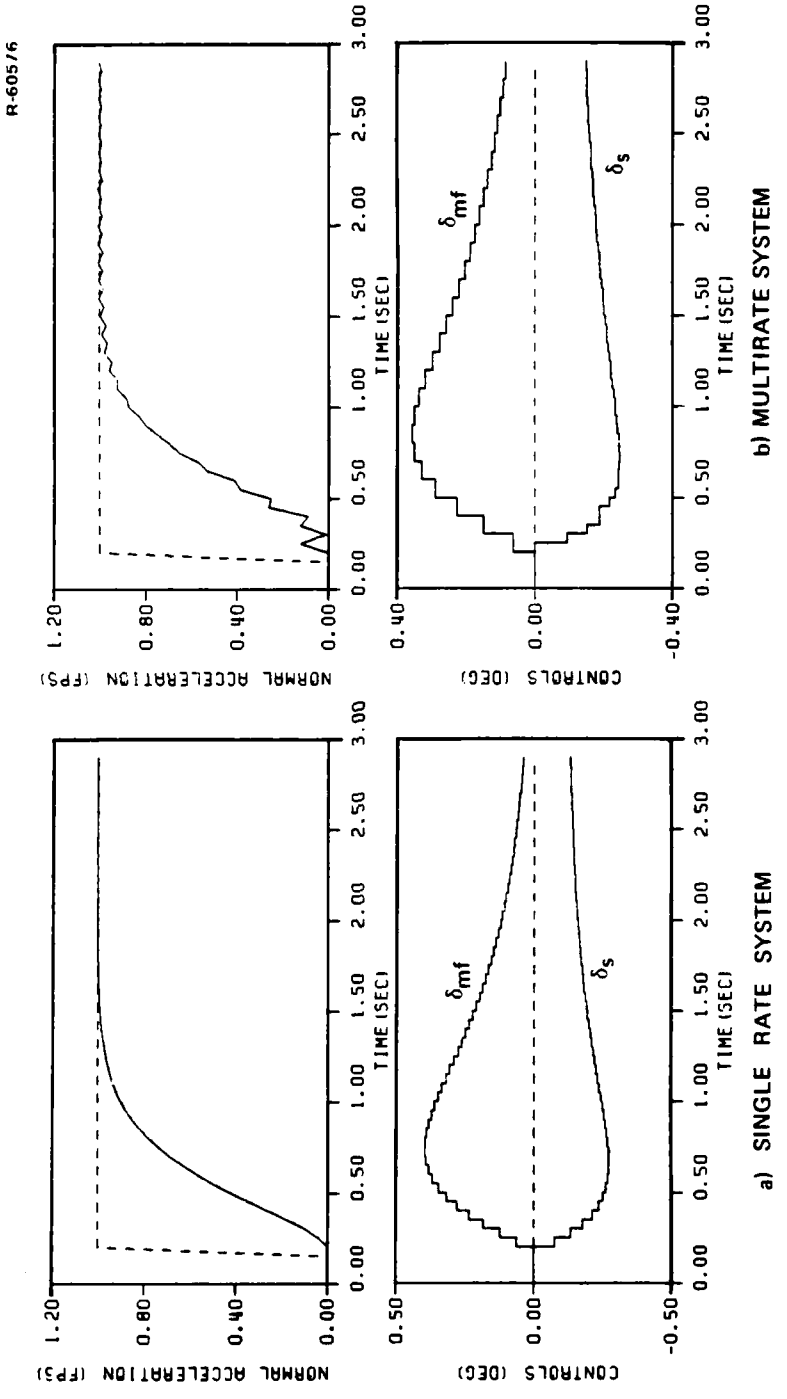

Figure 3.3-3 PI Controller Transient Responses (Longitudinal)

along with the histories of the longitudinal controls. The transient responses of the two control systems are very similar; each has a response time of roughly one second. The multirate system response "ratchets" at the initiation of the response and as the response approaches steady-state; this results from the lower computation rate of the maneuver flap and the fact that the stabilator skips a cycle in the control schedule (see Table 3.3-1). Since the longitudinal control deflections directly contribute to the value of normal acceleration, any roughness of their time histories due to low computation rate will show up in the normal acceleration response. If the ratcheting is unacceptable it could be eliminated substantially by using the explicit holding circuit implementation in Fig. 3.2-2 to smooth the response histories of stabilator and maneuver flap.

The primary lateral control mode response, stability axis roll rate, is shown in Fig. 3.3-4. The single rate and multirate controllers have identical responses; this is not surprising since roll rate is achieved primarily from differential stabilator deflection which is computed at the same rate for both systems. Since rudder angle is computed at a lower rate in the multirate system, differences in the lateral acceleration during the roll rate transient are expected. As shown in Fig. 3.3-4, the lateral acceleration response of the multirate system has the same peak value as the single rate system but lags the single-rate response by 0.2 sec. Also, some roughness of the lateral acceleration is evident in the multirate system response due to the lower computation rate of rudder deflections.

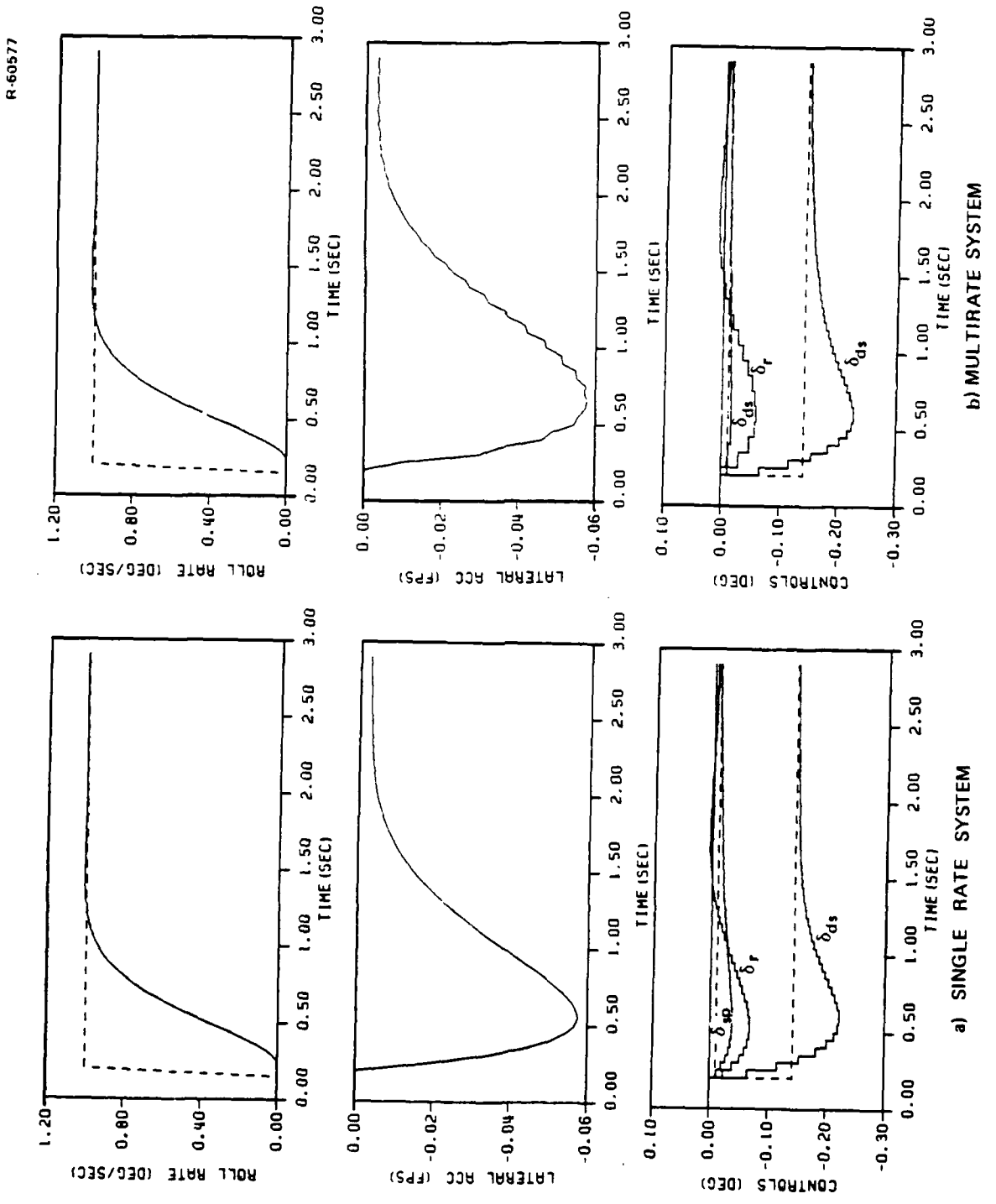

Figure 3.3-4 PI Controller Transient Responses (Lateral)

3.4 CHAPTER SUMMARY

Formulation and mathematical solution of the multirate proportional-plus-integral control synthesis problem has been presented. Two alternative formulations of the multirate PI controller are developed: one in which the low-rate controls are held between updates by the PI structure integrators and one in which additional holding circuit states are used to smooth low rate controls between updates.

Although the example PI designs presented in this chapter were derived from the same continuous-time cost functional matrices, the eigenvalues of the single rate and multirate systems differ. The differences in the eigenvalues are attributable to an approximation in the discrete-time representation of the augmented plant dynamics and variations of the optimization problem solution for the low-pass filtering portion of the control structure. The transient responses of the single rate and multirate systems are very similar; some rough response phenomena may be observed due to lower sample rates of secondary controls (e.g., maneuver flap, rudder). Although the eigenvalue variations and rough transient response phenomena are present in the multirate design, derivation of the multirate cost functional matrices from those of an acceptable single-rate system still offers a systematic design approach for multirate PI controllers.

4. ROBUSTNESS OF MULTIRATE DIGITAL CONTROL SYSTEMS

4.1 OVERVIEW

In the development of the multirate regulator and proportional-plus-integral controllers the primary design criteria were related to the transient response of the system; i.e., the multirate system should have the same transient response characteristics (response time, overshoot, etc.) as a specified continuous-time system. Since most flight control system specifications are written in terms of deterministic response characteristics (or frequency domain parameters such as natural frequency and damping ratio) the synthesis technique developed in the present study is a straightforward, systematic means of meeting system specifications in a multirate implementation.

The very important issue of relative stability, or, robustness, of the system may not be addressed if one designs only to specifications related to deterministic response characteristics. Robustness is quantified by many methods (e.g., phase/gain margins, disturbance rejection bandwidth) but generally represents some measure of the system's ability to resist disturbances and tolerate design uncertainties. Robustness is a very real concern in flight control applications. The designer never has exact knowledge of the vehicle aerodynamics or the flight condition; accordingly, the flight control system must be designed to tolerate uncertainties, remain stable, and perform within a specified range of handling qualities.

Evaluation of robustness requires an additional consideration in digital systems. Consider the situation of two digital state estimators for the same system operating at different sample rates. Figure 4.1-1 shows, heuristically, the effect of sample rate on the two estimators; the error variances of the estimator operating at the low sample rate (Fig. 4.1-1a) have a longer period of time to grow between measurement updates and, hence, are larger than those of the system operating at the higher sample rate (Fig. 4.1-1b). An analogous situation arises in controllers; the higher the sample rate, the less time for disturbance-induced errors to accumulate between control updates.

R-50840

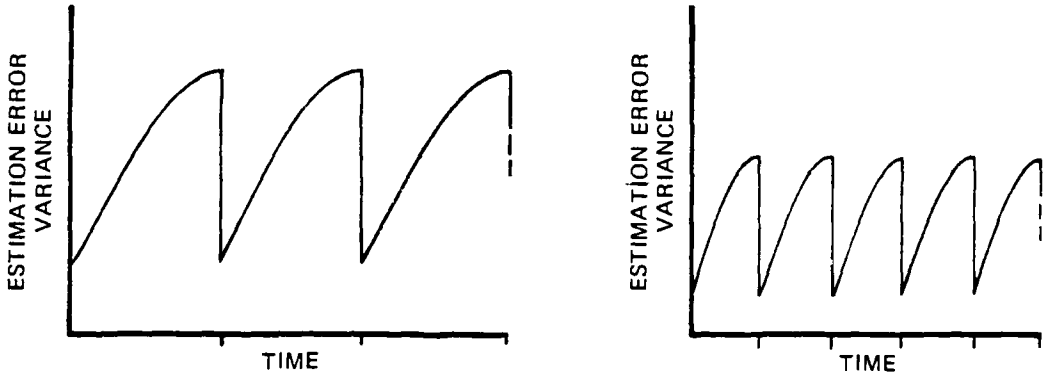

a) STANDARD SAMPLE RATE

b) INCREASED SAMPLE RATE

Figure 4.1-1 Error Covariance Histories of Two Single-Rate Estimators

Robustness evaluation takes on a further dimension in multirate digital systems. Consider, for example, the error variance history of roll angle for the example estimator of Section 2.5; Figure 2.5-2, which shows the error variance history of the example estimator, is repeated in Fig. 4.1-2. The error variance of roll angle varies on two time-scales: errors

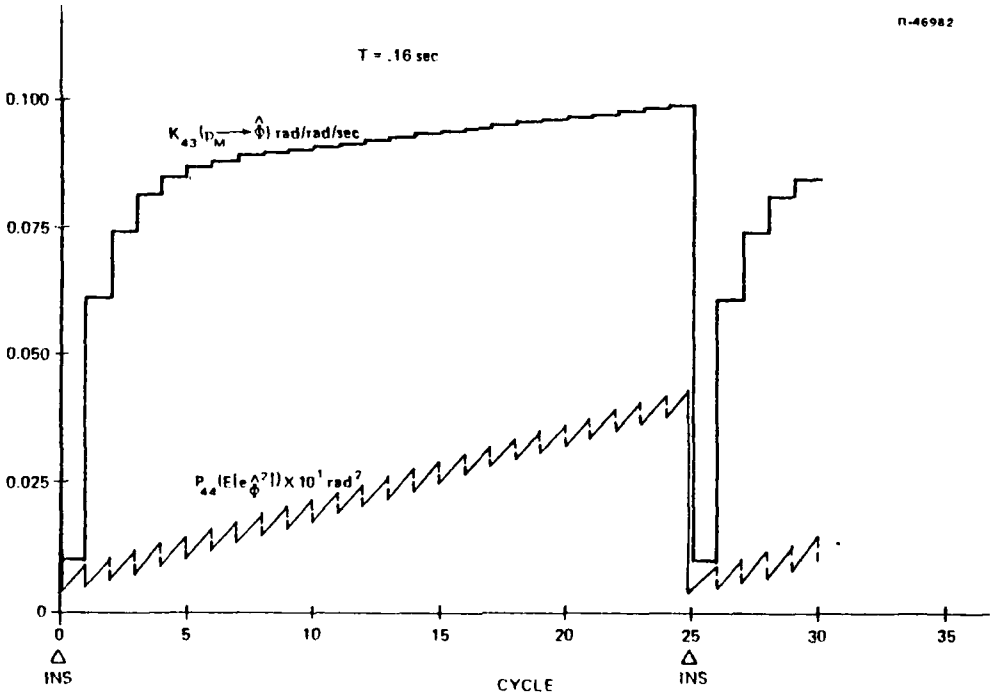

Figure 4.1-2 Roll Rate Gyro to Roll Angle Gain and Error Variance of Example Estimator

grow over a 25 cycle period between roll angle measurements and also in a "sawtooth" manner as the roll rate gyro measurements are used. Again, a similar situation exists in multirate control systems; errors may accumulate at multiple rates. Evaluation of error accumulation characteristics of multirate digital systems requires evaluation of the error variance history over a complete estimation/ control cycle.

A case study in robustness properties of a multirate flight control system is presented in this chapter. The example considered is the F-14 aircraft controlled by a multirate proportional-plus-integral (PI) controller. The aircraft/controller system is "flown" through a turbulent atmosphere; a covariance analysis of state variable errors determines the ability of the controller to reject turbulence-induced errors. The controller sample rate and control sequence are varied to determine

their influence on the disturbance rejection properties of the controller. Finally, a rudimentary proposal of a sample rate optimization scheme based on a robustness/computation tradeoff is presented.

The organization of this chapter is as follows: the mathematical formulation of the flight-through-turbulence dynamics and the corresponding error covariance equations is presented in Section 4.2. The results of the covariance analysis, considering variations of sample rate and control sequence, are presented in Section 4.3. The chapter is summarized in Section 4.4.

4.2 MATHEMATICAL FORMULATION

The mathematical models and covariance analysis technique used to evaluate the robustness of the multirate system are decribed in this section. The mathematical models of the aircraft and turbulence disturbances are outlined in Section 4.2.1; the controller and pilot model are described in Section 4.2.2; the covariance equations are derived in Section 4.2.3.

4.2.1 Vehicle/Disturbance Dynamics

The example vehicle is described in Chapter 3, i.e., the F-14 aircraft in trimmed level flight at an altitude of 20,000 ft and an airspeed of 183 m/sec (600 ft/sec).

The open-loop dynamics of the vehicle (including stability axis roll angle) are given by Eqs. 4.2-1 through 4.2-3. The dynamics matrix, F, is partitioned by columns and the turbulence-induced disturbances, v_g, r_g, and p_g, are added to the state vector on the right hand side of the equation.

$$\frac{d}{dt}\begin{bmatrix} v \\ r \\ p \end{bmatrix} = \begin{bmatrix} \underline{F}_v & \underline{F}_r & \underline{F}_p & \underline{F}_\phi \end{bmatrix} \begin{bmatrix} v+v_g \\ r+r_g \\ p+p_g \end{bmatrix} + G\underline{u} \qquad (4.2\text{-}1)$$

$$\dot{\phi} = p \cos\alpha + r \sin\alpha \qquad (4.2\text{-}2)$$

$$\underline{u}^T = (\delta_{sp}, \delta_{ds}, \delta_r) \qquad (4.2\text{-}3)$$

or, regrouping terms:

$$\dot{\underline{x}} = \tilde{F}\underline{x} + F_c\underline{x}_d + \tilde{G}\underline{u} \qquad (4.2\text{-}4)$$

$$\underline{x}^T = (v, r, p, \phi) \qquad (4.2\text{-}5)$$

$$\underline{x}_d^T = (v_g, r_g, p_g) \qquad (4.2\text{-}6)$$

with

$$\tilde{F} = \begin{bmatrix} & F & \\ \hline 0 & \sin\alpha & \cos\alpha & 0 \end{bmatrix} \qquad (4.2\text{-}7)$$

$$F_c = \begin{bmatrix} \underline{F}_v & \underline{F}_r & \underline{F}_p \\ 0 & 0 & 0 \end{bmatrix} \qquad (4.2\text{-}8)$$

$$\tilde{G} = \begin{bmatrix} G \\ \hline 0 \end{bmatrix} \qquad (4.2\text{-}9)$$

The dynamics of the lateral turbulence disturbances -- v_g, r_g, and p_g -- are determined from the Dryden turbulence spectra (Ref. 11). A second-order Markov model having an output spectrum equal to the Dryden spectrum of sideslip velocity is shown in Fig. 4.2-1; the state space realization of this model is given by Eq. 4.2-10.

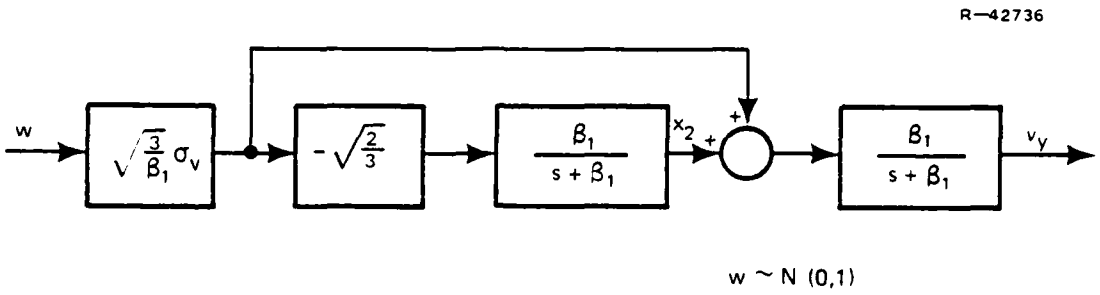

Figure 4.2-1 Sideslip Dynamics Realization

$$\frac{d}{dt}\begin{bmatrix} v \\ x_2 \end{bmatrix} = \begin{bmatrix} -\beta_1 & \beta_1 \\ 0 & -\beta_1 \end{bmatrix}\begin{bmatrix} v \\ x_2 \end{bmatrix} + \sqrt{\frac{3}{\beta_1}}\,\sigma_v \begin{bmatrix} \beta_1 \\ -\sqrt{\frac{2}{3}}\,\beta_1 \end{bmatrix} w \qquad (4.2\text{-}10)$$

$$w \sim N(0,1)$$

The output spectrum of this model is given by Eq. 4.2-11. The parameter transformations from the spatial frequency domain (i.e., turbulence scale, L_v, and wave number, Ω) to the temporal frequency domain are given by Eqs. 4.2-12 and 4.2-13. The spectrum parameters are listed in Table 4.2-1.

$$\Phi_{vv} = \sigma_v^2 \frac{V}{\beta_1 \pi}\,\beta_1^2\,\frac{(\beta_1^2 + 3\omega^2)}{(\beta_1^2 + \omega^2)^2} \qquad (4.2\text{-}11)$$

$$\beta_1 = \frac{V}{L_v} \qquad (4.2\text{-}12)$$

$$\omega = V\Omega \qquad (4.2\text{-}13)$$

The yaw rate disturbance is derived from the following relationship (Ref. 11):

$$r_g = -\frac{\partial v_g}{\partial x} \qquad (4.2\text{-}14)$$

where x is the longitudinal distance from the instantaneous c.g. position of the aircraft.

TABLE 4.2-1
SIDESLIP TURBULENCE PARAMETERS - DRYDEN MODEL

PARAMETER	DESCRIPTION	VALUE
σ_v	RMS sideslip velocity	5 ft/sec
V	Airspeed	600 ft/sec
L_v	Turbulence length scale	1750 ft
β_v	Spectrum break frequency	0.338 rad/sec
Ω	Spatial frequency (wave number)	variable
ω	Temporal frequency	variable

or

$$r_g = -\frac{1}{V}\frac{\partial v_g}{\partial t} \qquad (4.2\text{-}15)$$

Using the dynamic model for v_g:

$$r_g = -\frac{1}{V}\left\{-\beta_1 v_g + \beta_1 x_2 + \sqrt{\frac{3}{\beta_1}}\,\sigma_v \beta_1 w\right\} \qquad (4.2\text{-}16)$$

The spatial spectrum of the roll rate disturbance, p_g, is given by Eq. 4.2-17 (taken again from Ref. 11):

$$\Phi_{p_g}(\Omega) = \frac{\sigma_w^2}{L_w}\,\frac{0.8\left(\frac{\pi L_w}{4b}\right)^{1/3}}{1+\left[\left(\frac{4b}{\pi}\right)\Omega\right]^2} \qquad (4.2\text{-}17)$$

With the wingspan, b, equal to 64 ft (i.e., the F-14) and at an airspeed of 600 ft/sec, the temporal bandwidth of the roll rate spectrum is 7.25 rad/sec. Since the temporal bandwidth of the roll disturbance is roughly twenty times the bandwidth

of the sideslip disturbance, roll disturbance will be approximated as an uncorrelated (i.e., white) process in the dynamic analysis. The RMS value of the roll rate disturbance is given by Eq. 4.2-18.

$$E(p_g^2) = \left(\frac{\sigma_w^2 \pi}{L_w 8b}\right) 0.8 \left(\frac{\pi L_w}{b}\right)^{1/3} \tag{4.2-18}$$

with

$$L_w = 1750 \text{ ft} \tag{4.2-19}$$

$$\sigma_w = 5 \text{ ft/sec} \tag{4.2-20}$$

$$E(p_g^2) = 3.08\times10^{-4} \text{ rad}^2/\text{sec}^2 \tag{4.2-21}$$

or

$$\sigma_{p_g} = 0.7 \text{ deg/sec} \tag{4.2-22}$$

Combining the turbulence model dynamics with the vehicle dynamics, the following augmented system is obtained:

$$\dot{\underline{\hat{x}}} = \hat{F}\underline{\hat{x}} + G\underline{u} + \Lambda_d \underline{w} \tag{4.2-23}$$

with

$$\underline{\hat{x}}^T = (v, r, p, \phi, v_g, x_2) \tag{4.2-24}$$

$$w_i \sim N(0,1) \tag{4.2-25}$$

$$\hat{F} = \left[\begin{array}{c|c} \tilde{F} & \hat{F}_c \\ \hline 0 & F_d \end{array}\right] \tag{4.2-26}$$

$$\hat{G} = \begin{bmatrix} \tilde{G} \\ --- \\ 0 \end{bmatrix} \tag{4.2-27}$$

$$\hat{F}_c = \begin{bmatrix} (\underline{F}_v + \frac{\beta_1}{V}\underline{F}_r) & \frac{-\beta_1}{V}\underline{F}_r \\ 0 & 0 \end{bmatrix} \tag{4-2-28}$$

$$F_d = \begin{bmatrix} -\beta_1 & \beta_1 \\ 0 & -\beta_1 \end{bmatrix} \tag{4.2-29}$$

$$\Lambda_d = \begin{bmatrix} \frac{1}{V}\sqrt{\frac{3}{\beta_1}}\,\beta_1\,\underline{F}_r\sigma_v & \underline{F}_p\sigma_p \\ 0 & 0 \\ \sqrt{\frac{3}{\beta_1}}\,\beta_1\sigma_v & 0 \\ -\sqrt{\frac{2}{\beta_1}}\,\beta_1\sigma_v & 0 \end{bmatrix} \tag{4.2-30}$$

The discrete-time equivalent of the dynamics described by Eqs. 4.2-23 through 4.2-30 is:

$$\underline{\hat{x}}_{k+1} = \hat{\Phi}\underline{\hat{x}}_k + \hat{\Gamma}\underline{u}_k + \underline{w}_k \tag{4.2-31}$$

with

$$E(\underline{w}_k\underline{w}_k^T) = \int_0^{T_s} \hat{\Phi}(s)(\Lambda_d\Lambda_d^T)\hat{\Phi}(s)^T\,ds \tag{4.2-32}$$

$$= Q_d$$

4.2.2 Controller and Pilot Model

The controller used in this example is a multirate proportional-plus-integral (PI) controller designed to the same closed-loop specifications as the design example of Section 3.3. The control sample rates and sequencing are varied to determine their effect on the disturbance rejection performance of the system. Since the purpose of the controller, in this case, is to maintain a zero set point (i.e., trimmed level flight) as accurately as possible, the control law is implemented in its type-0 form; the feedback variable transformation to obtain a pure integration in the forward control path is not performed. The control law is implemented by Eq. 4.2-33.

$$\underline{u}_k = -T_s C_1 \underline{x}_{k-1} + (I - T_s C_2)\underline{u}_{k-1} \qquad (4.2\text{-}33)$$

The controller design regulates only the "inner loops"; i.e., sideslip velocity and angular rates are compensated by the controller. The regulation of the vehicle attitude is performed by the pilot (i.e., the pilot keeps the wings level). In this case, the pilot senses stability axis roll angle error and feeds back a roll rate command (i.e., lateral stick and rudder pedal inputs) proportional to the error. A pilot sensitivity of -1 (deg/sec)/deg was chosen for this example. Using the body axis roll and yaw rate dynamics and the stability axis roll rate equation (Eq. 4.2-2), pilot to differential stabilator and rudder gains were determined to produce -1 (deg/sec)/deg about the stability roll axis in steady-state; these gains are given by Eqs. 4.2-34 through 4.2-35.

$$K_p^T = (0,\ C_{p_{\delta_{ds}}},\ C_{p_{\delta_r}}) \qquad (4.2\text{-}34)$$

$$C_{p_{\delta_{ds}}} = 0.15 \text{ (deg/sec)/deg} \tag{4.2-35}$$

$$C_{p_{\delta_r}} = -0.018 \text{ (deg/sec)/deg} \tag{4.2-36}$$

In the next section, the vehicle and turbulence models are combined with the control functions described in this section to form an augmented closed-loop system. The disturbance rejection properties of this system are evaluated.

4.2.3 Covariance Analysis

The vehicle and turbulence models and the control functions described in Section 4.2.2 are combined into a single system given by:

$$\begin{bmatrix} \underline{x} \\ \underline{u} \\ \underline{x}_d \end{bmatrix}_{k+1} = \left[\begin{array}{c|c|c} \tilde{\Phi} & \Gamma & \Phi_c \\ \hline -T_s C_1 \;\; C_p & (I - T_s C_2) & 0 \\ \hline 0 & 0 & \Phi_d \end{array}\right]_k \begin{bmatrix} \underline{x} \\ \underline{u} \\ \underline{x}_d \end{bmatrix}_k + \underline{w}'_k \tag{4.2-37}$$

or

$$\underline{x}'_{k+1} = \Phi'_k \underline{x}'_k + w'_k \tag{4.2-38}$$

$$E(\underline{w}'_k \underline{w}'^{T}_k) = \left[\begin{array}{c|c|c} Q_{11} & 0 & Q_{12} \\ \hline 0 & 0 & 0 \\ \hline Q_{12}^T & 0 & Q_2{}^2 \end{array}\right] \tag{4.2-39}$$

$$= Q' \tag{4.2-40}$$

The partitions of the dynamics matrix in Eq. 4.2-37 are defined by Eq. 4.2-41.

$$\Phi' = \left[\begin{array}{cc|c|c} \multicolumn{2}{c|}{\text{vehicle dynamics}} & \text{control effectiveness} & \text{coupling} \\ \hline \text{proportional controls} & \text{pilot gains} & \text{low-pass controls} & 0 \\ \hline \multicolumn{2}{c|}{0} & 0 & \text{turbulence dynamics} \end{array}\right] \tag{4.2-41}$$

The $\tilde{\Phi}$, Φ_c, and Φ_d matrices are determined from partitions of the coupled vehicle/disturbance dynamics described in Section 4.2.1 (i.e., Eqs. 4.2-23 through 4.2-32).

$$\exp\left[\begin{array}{c|c} \tilde{F} & \hat{F}_c \\ \hline 0 & F_d \end{array}\right] = \left[\begin{array}{c|c} \tilde{\Phi} & \Phi_c \\ \hline 0 & \Phi_d \end{array}\right] \tag{4.2-42}$$

Similarly, the matrices Q_1, Q_2, and Q_{12} are defined by (see Eq. 4.2-32)

$$Q_d = \left[\begin{array}{c|c} Q_{11} & Q_{12} \\ \hline Q_{12}^T & Q_{22} \end{array}\right] \tag{4.2-43}$$

The discrete-time covariance equation for the augmented system given by Eqs. 4.2-38 and 4.2-40 is:

$$P_{k+1} = \Phi'_k P_k \Phi'^T_k + Q' \tag{4.2-44}$$

In steady-state, the solution of Eq. 4.2-44 is periodic with a period equal to the control schedule period, ℓ, i.e.:

$$P_{k+\ell} = P_k \tag{4.2-45}$$

Propagating Eq. 4.2-44 over ℓ cycles and using Eq. 4.2-45, one obtains:

$$P_k = \Phi^* P_k \Phi^{*T} + Q^* \tag{4.2-46}$$

where

$$\Phi^* = \Phi'_{k+\ell-1}\Phi'_{k+\ell-2} \cdots \Phi'_k \tag{4.2-47}$$

$$Q^* = \sum_{i=k+1}^{k+\ell-1} \Phi_i^* Q' \Phi_i^{*T} + Q' \tag{4.2-48}$$

$$\Phi_i^* = \Phi'_{k+\ell-1}\Phi'_{k+\ell-2} \cdots \Phi'_i \tag{4.2-49}$$

To determine the periodic steady-state solution to Eq. 4.2-44, the full-period covariance equation, Eq. 4.2-46, is solved; the remaining values of P_k over the complete control cycle are determined by propagating Eq. 4.2-44 for ℓ-1 cycles.

The mathematical formulation presented in this section was applied to the flight vehicle example. The results of this analysis are presented in the following section.

4.3 ROBUSTNESS EVALUATION

The mathematical formulation of Section 4.2 is applied to an example here. The sample rate and schedule of the controller described in Section 4.2.2 are varied to determine their effect on the disturbance rejection properties of the system.

The performance index for the control system is the sum of the stability-axis roll angle and sideslip angle covariances, i.e.:

$$J = P_{44} + P_{11}/V^2 \qquad (4.3\text{-}1)$$

This choice of performance index gives equal weighting to deviations from wings-level flight and undesired sideslipping (with attendant lateral acceleration). In the example considered here, periodicity of the covariance equation solution was observed. The variations of the variances of interest were in the fourth significant figure; for this case, a figure of merit based on average values of P_{11} and P_{44} is adequate.

The results of the covariance analysis/figure-of-merit computation for a matrix of differential stabilator-rudder schedules is presented in Fig. 4.3-1. Here the base sample rate is 40 Hz (T_p = 0.025 sec) and the control period is 8 cycles (0.2 sec). As shown in the figure, the three curves indicate the performance of the system for three rates of differential stabilator computation (i.e., number of differential stabilator computations every 8 cycles) as a function of rudder computation rate. In all cases, reducing the number of rudder computations performed during the 8 cycle period increases the performance index; this is primarily due to the increase in sideslip covariance as the rudder rate is reduced. Similarly, as the number of differential stabilator computations is reduced the covariance of roll angle error increases thereby increasing the performance index.

A potential trade-off of performance and computational load can be identified at this point. Suppose that it is desired that the performance index have a value of 0.8 deg^2 or less (indicated by the dotted line in Fig. 4.3-1). The cross-

R-60619

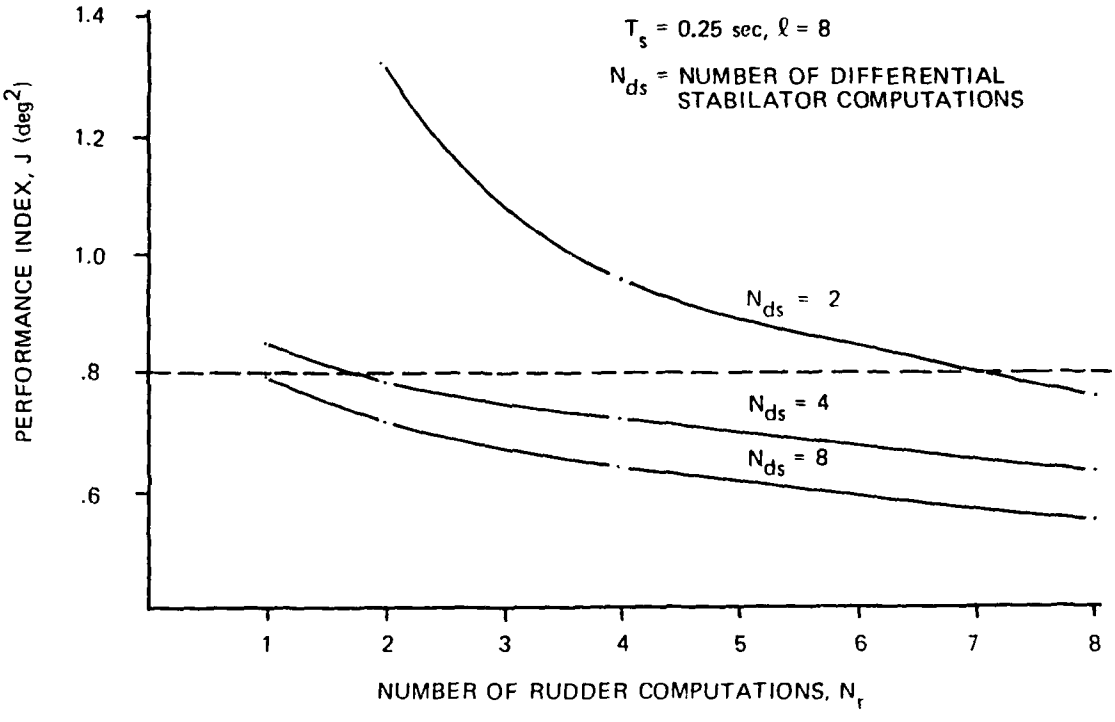

Figure 4.3-1 Performance of Multirate System as a Function of Control Sequence

plot of J=0.8 deg^2 into a N_{ds}/N_r axis system is shown in Fig. 4.3-2. Since each differential stabilator or rudder control computation "costs" the same (i.e., each involves the same number of multiplications and additions per computation) curves of constant computational burden can be represented by the dashed straight lines plotted in Fig. 4.3-2. The tangent intersection of the N_t = 6 line with the J = 0.8-deg^2 curve indicates that the desired performance can be achieved with the minimum number of computations if the control schedule includes 4 differential stabilator and 2 rudder computations per 8-cycle period.

Here for a desired level of system performance a graphical technique is used to optimize the sampling policy

R-60618

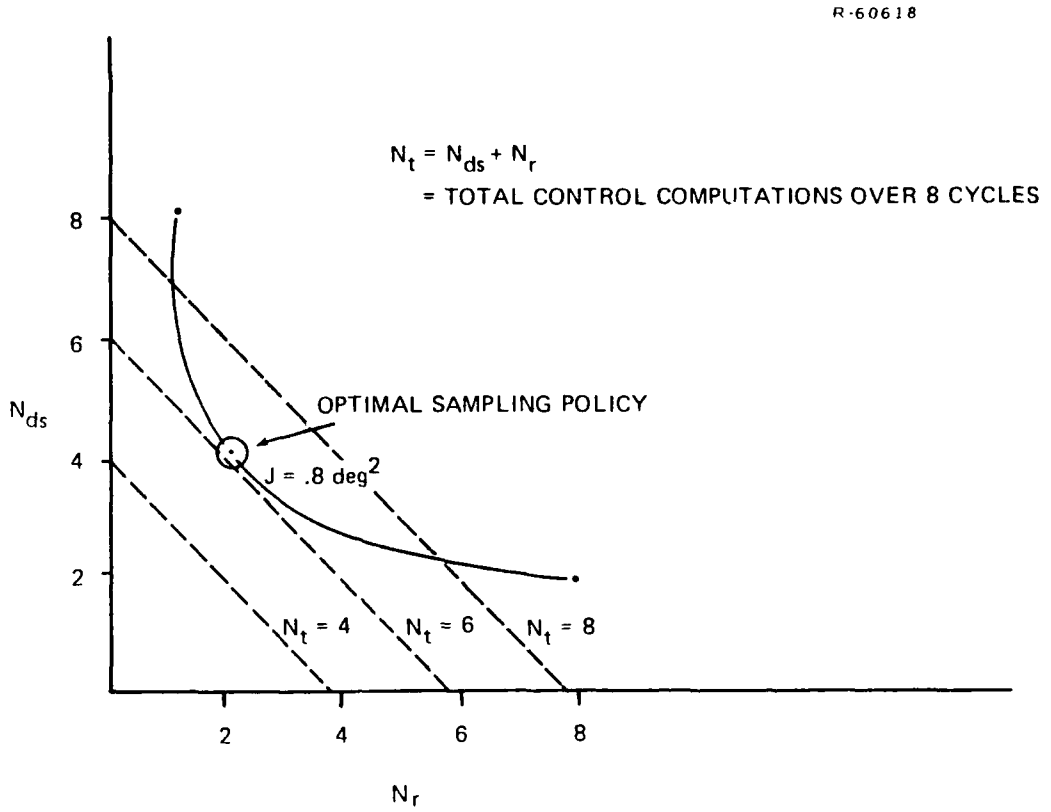

Figure 4.3-2 Sampling Policy Optimization for a Fixed Level of Performance

(i.e., minimize the number of computations). In aircraft control applications, the sample rate optimization problem is posed differently; the computational budget is fixed and the designer endeavors to optimize system performance within this budget. A graphical conception of the performance optimization problem is shown in Fig. 4.3-3. The computation budget is represented by a single straight line; the optimal sclution is the tangent intersection of the highest performance level curve with the computation budget line.

The graphical methods of performance/computation optimization described here can be cast into a general mathematical optimization framework. The development of such a general mathematical technique is discussed in Chapter 5.

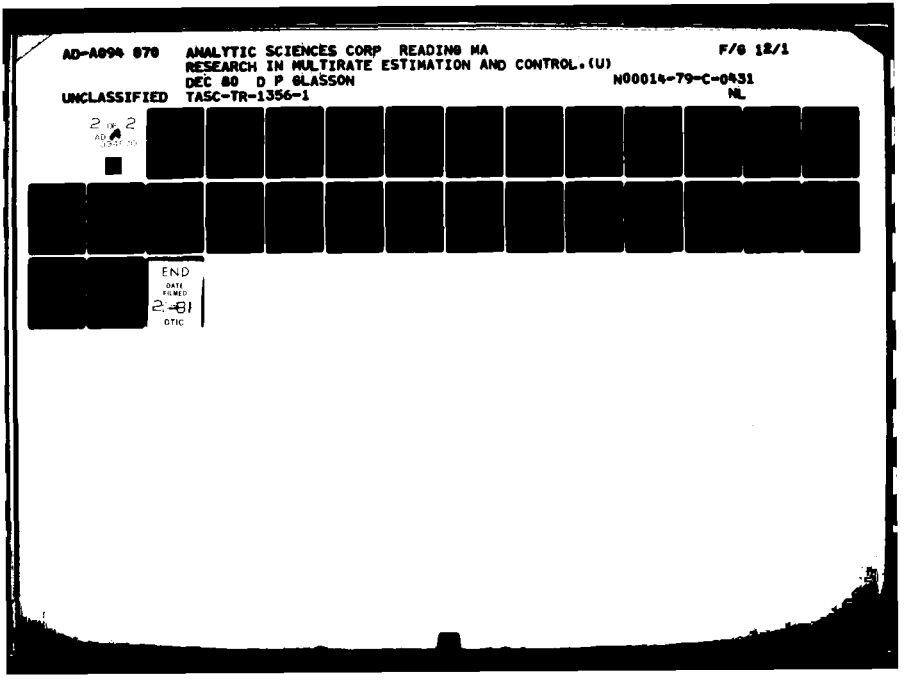
AD-A094 070
ANALYTIC SCIENCES CORP READING MA
F/G 12/1
RESEARCH IN MULTIRATE ESTIMATION AND CONTROL.(U)
DEC 80 D P GLASSON
N00014-79-C-0431
UNCLASSIFIED
TASC-TR-1356-1
NL
2 OF 2
END
DATE FILMED
2-81
DTIC

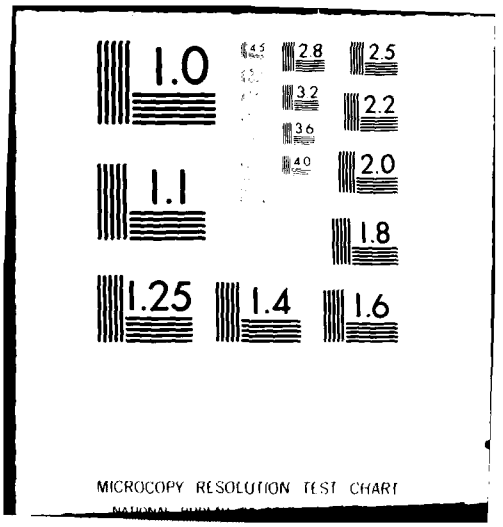
1.0
2.8
2.5
3.2
2.2
3.6
4.0
2.0
1.1
1.8
1.25
1.4
1.6
MICROCOPY RESOLUTION TEST CHART

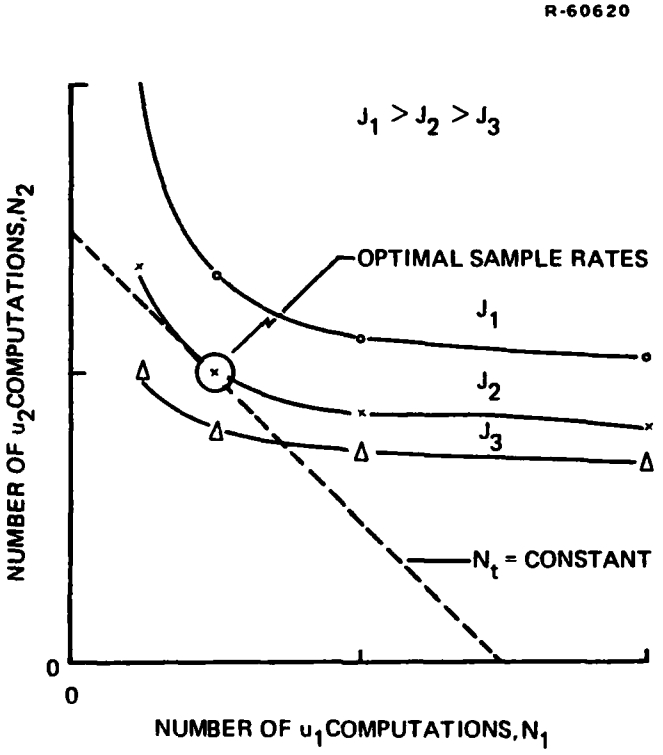

Figure 4.3-3 Performance Optimization for a Fixed Computation Budget

4.4 CHAPTER SUMMARY

In this chapter a methodology for evaluating the robustness of a multirate system is presented. This methodology is based on steady-state covariance analysis of the multirate system with variations of control schedule to determine disturbance rejection sensitivity to control computation rates.

The control error covariance of a multirate system is periodic in steady-state with a period equal to the control schedule period. The periodic history of the steady-state covariance solution is obtained by constructing and solving a Liapunov equation which represents the full control period

covariance dynamics (Eq. 4.2-46), then propagating the cycle-to-cycle covariance equation (Eq. 4.2-44) over the control period.

The robustness of an example multirate system is evaluated as a function of control scheduling. As expected, the disturbance rejection performance of the example system is degraded by lower sample rates of the controls. An approach for optimization of the performance/computation tradeoff is presented; this approach can be cast in a general mathematical optimization framework.

5. CONCLUSIONS AND RECOMMENDATIONS

This report presents new techniques for the synthesis and analysis of multirate estimation and control algorithms with applications to flight control system design. Topics addressed in this report include multirate state estimator and controller design, design of multirate proportional-plus-integral controllers, eigen-analysis of multirate systems, and robustness of multirate control systems.

5.1 CONCLUSIONS

This investigation provides the following significant results:

- Optimal Multirate Estimator - The optimal multirate estimator is characterized by periodically time-varying gains having a period equal to the number of discrete time-steps over which the measurement schedule repeats itself. The error covariance of the multirate estimator varies over the measurement schedule and also from cycle-to-cycle as high-rate measurements are used to improve extrapolations.
- Optimal Multirate Regulator - A systematic procedure for synthesizing optimal multirate regulators is developed. This procedure produces a multirate regulator which minimizes the same performance index used to design a continuous-time regulator which meets desired specifications. The present technique also obviates dimensionality problems typically encountered in applying classically-based techniques to multirate systems.

- Proportional-Plus-Integral Controller - The multirate regulator synthesis procedure is extended to the proportional-plus-integral (PI) control structure. Again, the design procedure prescribed here produces a multirate PI controller which optimizes the same cost functional as a prescribed continuous-time system.

- Robustness of Multirate Controllers - A covariance analysis methodology for evaluating the disturbance rejection properties of multirate control systems is developed. This technique is applied to a flight control example; the trend of reduced resistance to disturbances with lower sample rates of the controls is quantified by this technique.

- Sample Rate Optimization - A solution to optimization of the performance/computation tradeoff is demonstrated graphically. For a given level of performance, a control schedule that minimizes the rate of control computations is determined.

5.2 RECOMMENDATIONS

It is recommended that the following studies related to the present investigation be undertaken.

- Mathematically formulate the sample rate optimization problem. Develop an algorithm to solve this problem for the general multirate controller. Investigate the properties of the optimal solution through a design example.

- Investigate the related field of perturbation methods (i.e., system decomposition by scaling fast and slow dynamics). Determine benefits of incorporating perturbation methods in the multirate design process; a specific area of application would be in active control of vehicle flexibility modes.

- Application of the techniques developed in this report to a practical flight control system implementation.

APPENDIX A
MATHEMATICAL DERIVATION OF MULTIRATE REGULATOR WEIGHTING MATRICES

In this appendix derivations of the weighting matrices for the multirate regulator design are presented. The intent is to determine the weighting matrices for the multirate design that will yield a cost functional equivalent to that of a specified continuous-time design. The approach is to modify appropriately the continuous-time matrices to account for the addition of the slow control holding circuit, then use these matrices along with the discrete-time dynamics of the augmented plant to derive the discrete-time weighting matrices.

The development shows that the weighting matrices for the multirate design can be constructed from partitions of the single-rate (high rate) weighting matrices (as was described in Section 2.3). In order that the constitutent partitions of the multirate matrices can be readily recognized, the single-rate wieghting matrices and their appropriate partitions are derived in Section A.1. The multirate matrices are derived in Section A.2; the partition correspondence of the single-rate and multirate matrices is also indicated.

A.1 SINGLE-RATE WEIGHTING MATRIX DERIVATION AND PARTITIONING

Before applying the relationships of Ref. 5 to derive the multirate weighting matrices, the single rate control weighting and state-control cross-weighting matrices are derived and partitioned. To this end, Eqs. 2.3-21 and 2.3-22 are expanded.

$$\bar{R} = RT_s + \int_0^{T_s} \Gamma^T Q \Gamma dt \qquad \text{(A.1-1)}$$

with

$$R = \begin{bmatrix} R_f & 0 \\ 0 & R_s \end{bmatrix} \qquad \text{(A.1-2)}$$

$$\bar{R} = T_s \begin{bmatrix} R_f & 0 \\ 0 & R_s \end{bmatrix} + \int_0^{T_s} \begin{pmatrix} \Gamma_f^T \\ \Gamma_s^T \end{pmatrix} Q \, (\Gamma_f \; \Gamma_s) dt \qquad \text{(A.1-3)}$$

$$= \begin{bmatrix} T_s R_f & 0 \\ 0 & T_s R_s \end{bmatrix} + \int_0^{T_s} \begin{bmatrix} \Gamma_f^T Q \Gamma_f & \Gamma_f^T Q \Gamma_s \\ \Gamma_s^T Q \Gamma_f & \Gamma_s^T Q \Gamma_s \end{bmatrix} dt \qquad \text{(A.1-4)}$$

$$= \begin{bmatrix} \bar{R}_f & \bar{R}_{sf}^T \\ \bar{R}_{sf} & \bar{R}_s \end{bmatrix} \qquad \text{(A.1-5)}$$

$$\bar{M} = \int_0^{T_s} \phi^T Q (\Gamma_f \mid \Gamma_s) dt \qquad \text{(A.1-6)}$$

$$= \int_0^{T_s} [\phi^T Q \Gamma_f \mid \phi^T Q \Gamma_s] dt \qquad \text{(A.1-7)}$$

$$= [\bar{M}_f \mid \bar{M}_s] \qquad \text{(A.1-8)}$$

As the following development shows, the multirate weighting matrices can be constructed using the partitioned single rate matrices, Eqs. A.1-5 and A.1-8.

A.2 MULTIRATE WEIGHTING MATRIX DERIVATION

The first step in deriving the multirate weighting matrices is to modify the continuous time weighting matrices, Q and R, to account for holding circuit state augmentation. The modified forms of the continuous-time weighting matrices are determined by considering the equivalent continuous-time dynamics of the augmented system, Eq. 2.3-23:

$$\begin{bmatrix} \dot{\underline{x}} \\ --- \\ \dot{\underline{u}}_s \end{bmatrix} = \left[\begin{array}{c|c} F & G_s \\ \hline 0 & 0 \end{array}\right] \begin{bmatrix} \underline{x} \\ --- \\ \underline{u}_s \end{bmatrix} + \left[\begin{array}{c|c} G_f & 0 \\ \hline 0 & I\delta(t-i\ell T_s) \end{array}\right] \begin{bmatrix} \underline{u}_f \\ --- \\ \underline{v} \end{bmatrix} \qquad \text{(A.2-1)}$$

Here the slow control holding circuit is represented as an integrator; the impulse function, $\delta(t-i\ell T_s)$, in the augmented control effectiveness matrix allows the increment function, $\underline{v}$, to make discontinuous changes in $\underline{u}_s$ at $t = i\ell T$. If the continuous-time control weighting matrix for the non-augmented system Eq. 2.3-8 is restricted to the form

$$R = \left[\begin{array}{c|c} R_f & 0 \\ \hline 0 & R_s \end{array}\right] \qquad \text{(A.2-2)}$$

(i.e., no cross-weighting of $\underline{u}_f$ and $\underline{v}_s$) the weighting matrices of the augmented continuous-time system are:

$$\tilde{Q} = \left[\begin{array}{c|c} Q & 0 \\ \hline 0 & R_s \end{array}\right] \tag{A.2-3}$$

$$\tilde{R} = \left[\begin{array}{c|c} R_f & 0 \\ \hline 0 & 0 \end{array}\right] \tag{A.2-4}$$

The cost functional constructed from $\tilde{Q}$ and $\tilde{R}$ is identical to that of the non-augmented system, Eq. 2.3-9 (as is desired); i.e.:

$$J = \frac{1}{2}\int_0^\infty \left\{ (\underline{x}^T, \underline{u}_s^T) \left[\begin{array}{c|c} Q & 0 \\ \hline 0 & R_s \end{array}\right] \left(\begin{array}{c} \underline{x} \\ \hline \underline{u}_s \end{array}\right) + (\underline{u}_f^T, \underline{v}^T) \left[\begin{array}{c|c} R_f & 0 \\ \hline 0 & 0 \end{array}\right] \left(\begin{array}{c} \underline{u}_f \\ \hline \underline{v} \end{array}\right) \right\} dt \tag{A.2-5}$$

$$= \frac{1}{2}\int_0^\infty \left\{ \underline{x}^T Q \underline{x} + \underline{u}_s^T R_s \underline{u}_s + \underline{u}_f^T R_f \underline{u}_f \right\} dt \tag{A.2-6}$$

$$= \frac{1}{2}\int_0^\infty \left\{ \underline{x}^T Q \underline{x} + \underline{u}^T R \underline{u} \right\} dt \tag{A.2-7}$$

Note that $\tilde{R}$ assigns no penalty to $\underline{v}$; the control $\underline{u}_s$ is penalized, but discontinuous changes in $\underline{u}_s$ are not penalized.

The multirate cost-functional matrices -- $\hat{Q}$, $\hat{M}$, $\hat{R}$ -- used in Eqs. 2.3-24 through 2.3-30 are now derived using Eqs. A.2-3 and A.2-4. The multirate augmented state weighting matrix is time-invariant; it is derived as follows:

$$\hat{Q} = \int_0^{T_s} \hat{\Phi}^T \tilde{Q} \hat{\Phi} dt \qquad \text{(A.2-8)}$$

$$= \int_0^{T_s} \left[\begin{array}{c|c} \Phi^T & 0 \\ \hline \Gamma_s^T & I \end{array}\right] \left[\begin{array}{c|c} Q & 0 \\ \hline 0 & R_s \end{array}\right] \left[\begin{array}{c|c} \Phi & \Gamma_s \\ \hline 0 & I \end{array}\right] dt$$

(A.2-9)

$$= \int_0^{T_s} \left[\begin{array}{c|c} \Phi^T Q \Phi & \Phi^T Q \Gamma_s \\ \hline \Gamma_s^T Q \Phi & \Gamma_s^T Q \Gamma_s + R_s \end{array}\right] dt \qquad \text{(A.2-10)}$$

$$\hat{Q} = \left[\begin{array}{c|c} \bar{Q} & \bar{M}_s \\ \hline \bar{M}_s^T & \bar{R}_s \end{array}\right] \qquad \text{(A.2-11)}$$

The $\hat{R}$ and $\hat{M}$ matrices vary (in dimension) depending on whether or not both fast and slow controls are being updated on a particular cycle. On a cycle when both controls are updated (i.e., a major update), the following relationships for $\hat{R}$ and $\hat{M}$ are applied:

$$\hat{R}_{i\ell} = T_s \left[\begin{array}{c|c} R_f & 0 \\ \hline 0 & 0 \end{array}\right] + \int_0^{T_s} \left[\begin{array}{c|c} \Gamma_f^T & 0 \\ \hline \Gamma_s^T & I \end{array}\right] \left[\begin{array}{c|c} Q & 0 \\ \hline 0 & R_s \end{array}\right] \left[\begin{array}{c|c} \Gamma_f & \Gamma_s \\ \hline 0 & I \end{array}\right] dt$$

(A.2-12)

$$= \int_0^{T_s} \left[\begin{array}{c|c} R_f + \Gamma_f^T Q \Gamma_f & \Gamma_f^T Q \Gamma_s \\ \hline \Gamma_s^T Q \Gamma_f & R_s + \Gamma_s^T Q \Gamma_s \end{array}\right] dt \qquad \text{(A.2-13)}$$

$$\boxed{\hat{R}_{i\ell} = \bar{R}} \qquad \text{(A.2-14)}$$

$$\hat{M}_{i\ell} = \int_0^{T_s} \left[\begin{array}{c|c} \Phi^T & 0 \\ \hline \Gamma_s^T & I \end{array}\right] \left[\begin{array}{c|c} Q & 0 \\ \hline 0 & R_s \end{array}\right] \left[\begin{array}{c|c} \Gamma_f & \Gamma_s \\ \hline 0 & I \end{array}\right] dt \qquad \text{(A.2-15)}$$

$$= \int_0^{T_s} \left[\begin{array}{c|c} \Phi^T Q \Gamma_f & \Phi^T Q \Gamma_f \\ \hline \Gamma_s^T Q \Gamma & R_s + \Gamma_s^T Q \Gamma_f \end{array}\right] dt \qquad \text{(A.2-16)}$$

$$\boxed{\hat{M}_{i\ell} = \left[\begin{array}{c|c} \bar{M}_f & \bar{M}_s \\ \hline \bar{R}_{sf} & \bar{R}_s \end{array}\right]} \qquad \text{(A.2-17)}$$

On cycles when only the fast control is updated (i.e., a subinterval), the order of the control vector is reduced, i.e.:

$$\underline{u} = \underline{u}_f \qquad \text{(A.2-18)}$$

$$\hat{\Gamma}_k = \left[\begin{array}{c} \Gamma_f \\ \hline 0 \end{array}\right] \qquad \text{(A.2-19)}$$

Accordingly, the following expressions for $\hat{R}$ and $\hat{M}$ are obtained by truncating Eqs. A.2-14 and A.2-17.

$$\boxed{\hat{R}_k = \bar{R}_f} \tag{A.2-20}$$

$$\boxed{\hat{M}_k = \begin{bmatrix} \bar{M}_f \\ --- \\ \bar{R}_{sf} \end{bmatrix}} \tag{A.2-21}$$

As Eqs. A.2-14, A.2-17, A.2-20, and A.2-21 indicate, the $\hat{Q}$, $\hat{M}$, and $\hat{R}$ matrices for the multirate design can be constructed from appropriate partitions of the equivalent single rate weighting matrices: $\bar{Q}$, $\bar{M}$, and $\bar{R}$. This method of weighting matrix construction is very advantageous since software packages to compute the single rate weighting matrices are already in common usage. Again, the regulator derived from these matrices has identical transient response characteristics to the single-rate and continuous-time systems.

APPENDIX B
MATRICES FOR EXAMPLE MULTIRATE SYSTEM

The matrices used in the example estimation/control system design of Section 2.5 are listed here*. The notation of Sections B.1, B.2, and B.3 corresponds to that used in Sections 2.5.1, 2.5.2, and 2.5.3, respectively.

B.1 PLANT/MEASUREMENT DESCRIPTION

Discrete System Dynamics:

$$\Phi = \begin{bmatrix} 0.9904E\ 00 & -0.1585E\ 00 & 0.3279E\text{-}01 & 0.3504E\text{-}02 \\ -0.4447E\text{-}01 & 0.9970E\ 00 & 0.5580E\text{-}04 & -0.6688E\text{-}04 \\ -0.4033E\ 00 & 0.5021E\text{-}01 & 0.9465E\ 00 & -0.1393E\text{-}02 \\ -0.3256E\text{-}01 & 0.3173E\text{-}02 & 0.1559E\ 00 & 0.9999E\ 00 \end{bmatrix} \quad \text{(B.1-1)}$$

Fast Control Effectiveness (Aileron):

$$\Gamma_f = \begin{bmatrix} 0.6087E\text{-}02 \\ 0.1942E\text{-}02 \\ 0.3727E\ 00 \\ 0.3009E\text{-}01 \end{bmatrix} \quad \text{(B.1-2)}$$

*The numerical values presented here are given in standard "E format"; the notation EsNN indicates a factor of 10^{sNN}. For example, 0.1000E-02 is equivalent to 0.001.

Slow Control Effectiveness (Rudder):

$$\Gamma_s = \begin{bmatrix} 0.4976E\text{-}02 \\ -0.2632E\text{-}01 \\ 0.1304E\ 00 \\ 0.1054E\text{-}01 \end{bmatrix} \qquad \text{(B.1-3)}$$

Process Noise Covariance:

$$Q = \begin{bmatrix} 0.4002E\ 01 & -0.4115E\ 00 & -0.7548E\ 00 & -0.3688E\text{-}01 \\ -0.4115E\ 00 & 0.3987E\ 01 & 0.1053E\ 00 & 0.5245E\text{-}02 \\ -0.7548E\ 00 & 0.1053E\ 00 & 0.4023E\ 01 & 0.3173E\ 00 \\ -0.3689E\text{-}01 & 0.5245E\text{-}02 & 0.3173E\ 00 & 0.3372E\text{-}01 \end{bmatrix}$$

(B.1-4)

B.2 MULTIRATE KALMAN FILTER

High Rate Measurement Sensitivity:

$$H_f = \begin{bmatrix} -0.1020E\ 01 & -0.1318E\text{-}02 & -0.5319E\ 01 & 0.5620E\ 00 \\ 0.0000E\ 01 & 0.1000E\ 01 & 0.0000E\ 01 & 0.0000E\ 01 \\ 0.0000E\ 01 & 0.0000E\ 01 & 0.1000E\ 01 & 0.0000E\ 01 \end{bmatrix}$$

(B.2-1)

INS Measurement Sensitivity:

$$H_s = (0.0000E\ 01 \quad 0.0000E\ 01 \quad 0.0000E\ 01 \quad 0.1000E\ 01)$$

(B.2-2)

High Rate Measurement Noise:

$$R_f = \begin{bmatrix} 0.4000E\ 01 & 0.0000E\ 01 & 0.0000E\ 01 \\ 0.0000E\ 01 & 0.2500E\ 00 & 0.0000E\ 01 \\ 0.0000E\ 01 & 0.0000E\ 01 & 0.2500E\ 00 \end{bmatrix} \qquad \text{(B.2-3)}$$

INS Measurement Noise:

$$R_s = 0.4000E\text{-}01 \qquad \text{(B.2-4)}$$

B.3 MULTIRATE REGULATOR DESIGN

Continuous-time State Weighting Matrix:

$$Q = \begin{bmatrix} 0.1000E\text{-}01 & 0.0 & 0.0 & 0.0 \\ 0.0 & 0.2500E\text{-}02 & 0.0 & 0.0 \\ 0.0 & 0.0 & 0.2500E\text{-}02 & 0.0 \\ 0.0 & 0.0 & 0.0 & 0.4000E\text{-}01 \end{bmatrix} \qquad \text{(B.3-1)}$$

Continuous-time Control Weighting Matrix:

$$R = \begin{bmatrix} 0.2500E\ 00 & 0.0 \\ 0.0 & 0.2500E\ 00 \end{bmatrix} \qquad \text{(B.3-2)}$$

Discrete-time State Weighting Matrix (Single Rate):

$$Q = \begin{bmatrix} 0.1610E\text{-}02 & -0.1378E\text{-}03 & -0.6053E\text{-}04 & -0.6694E\text{-}04 \\ -0.1378E\text{-}03 & 0.4120E\text{-}03 & 0.5617E\text{-}05 & 0.5552E\text{-}05 \\ -0.6053E\text{-}04 & 0.5617E\text{-}05 & 0.4330E\text{-}03 & 0.5033E\text{-}03 \\ -0.6694E\text{-}04 & 0.5552E\text{-}05 & 0.5033E\text{-}00 & 0.6400E\text{-}02 \end{bmatrix} \qquad \text{(B.3-3)}$$

Discrete-time Control-State Cross Product Matrix (Single Rate):

$$M = \begin{bmatrix} -0.4594E\text{-}03 & 0.2006E\text{-}02 \\ -0.1166E\text{-}03 & 0.7041E\text{-}03 \\ 0.5571E\text{-}04 & 0.1610E\text{-}02 \\ -0.1199E\text{-}03 & 0.5649E\text{-}03 \end{bmatrix} \qquad \text{(B.3-4)}$$

Discrete-time Control Weighting Matrix (Single Rate):

$$R = \begin{bmatrix} 0.4002E\text{-}01 & 0.6988E\text{-}05 \\ 0.6988E\text{-}05 & 0.4002E\text{-}01 \end{bmatrix} \qquad (B.3\text{-}5)$$

APPENDIX C
NEWTON'S METHOD SOLUTION OF THE PERIODIC RICATTI EQUATION

A method for finding the steady-state solution of the periodic Ricatti equation of multirate control design is presented in this appendix. The Liapunov equation derivation presented here is a revised development of an original derivation in Ref. 1; the starting solution algorithm was developed as part of the present research activity.

It is desired to determine the periodic steady-state solution to Eqs. 2.3-26 and 2.3-27:

$$\hat{L}_k = (\hat{\Gamma}_k^T \hat{P}_{k+1} \hat{\Gamma}_k + \hat{R}_k)^{-1} \hat{\Gamma}_k^T \hat{P}_{k+1} \tag{2.3-26}$$

$$\hat{P}_k = \hat{\theta}_k^T (I - \hat{L}_k^T \hat{\Gamma}_k^T) \hat{P}_{k+1} \hat{\theta}_k + \hat{Q}_k^* \tag{2.3-27}$$

where $\hat{\theta}_k$ and $\hat{Q}_k^*$ are as defined by Eqs. 2.3-28 and 2.3-29.

Equation 2.3-27 can be written in the form

$$\hat{P}_k = \hat{\theta}_k^T (I - \hat{L}_k^T \hat{\Gamma}_k^T) \hat{P}_{k+1} (I - \hat{\Gamma}_k \hat{L}_k) \hat{\theta}_k + \hat{\theta}_k^T (I - \hat{L}_k^T \hat{\Gamma}_k^T) \hat{P}_{k+1} \hat{\Gamma}_k \hat{L}_k \hat{\theta}_k + \hat{Q}_k^* \tag{C-1}$$

and Eq. 2.3-26 as:

$$(\hat{\Gamma}_k^T \hat{P}_{k+1} \hat{\Gamma}_k + \hat{R}_k)\hat{L}_k = \hat{\Gamma}_k^T \hat{P}_{k+1} \qquad \text{(C-2)}$$

Substituting Eq. C-2 into the second term on the right hand side of Eq. C-1, the following form of the Ricatti equation is obtained:

$$\hat{P}_k = \hat{\theta}_k^T (I - \hat{\Gamma}_k \hat{L}_k)^T \hat{P}_{k+1} (I - \hat{\Gamma}_k \hat{L}_k)\hat{\theta}_k + \hat{L}_k^T \hat{R}_k \hat{L}_k + \hat{Q}_k^* \qquad \text{(C-3)}$$

or

$$\hat{P}_k = \bar{\theta}_k^T \hat{P}_{k+1} \bar{\theta}_k + \bar{Q}_k \qquad \text{(C-4)}$$

with

$$\bar{\theta}_k = (I - \hat{\Gamma}_k \hat{L}_k)\hat{\theta}_k \qquad \text{(C-5)}$$

$$\bar{Q}_k = \hat{Q}_k^* + \hat{L}_k^T \hat{R}_k \hat{L}_k \qquad \text{(C-6)}$$

Propagating Eq. C-4 backwards in time from cycle $k=\ell$ to cycle $k=0$ and using the property that in steady-state:

$$\hat{P}_0 = \hat{P}_\ell \qquad \text{(C-7)}$$

one obtains:

$$\hat{P}_\ell = \theta^{*T} \hat{P}_\ell \theta^* + Q^* \qquad \text{(C-8)}$$

where

$$\theta^* = \bar{\theta}_{\ell-1} \bar{\theta}_{\ell-2} \cdots \bar{\theta}_0 \qquad \text{(C-9)}$$

$$Q^* = Q_1 + \sum_{k=0}^{\ell-2} \bar{\theta}_k^T \bar{\theta}_{k+1}^T \cdots \bar{\theta}_{(\ell-2)-k}^T \bar{Q}_{(\ell-1)-k} \bar{\theta}_{(\ell-2)-k} \cdots \bar{\theta}_{k+1} \bar{\theta}_k$$

The periodic steady-state solution of the multirate control Ricatti equation can be obtained by iteratively solving the Liapunov equation given by Eq. C-8 to find $\hat{P}_\ell$, then stepping through Eqs. 2.3-26 and 2.3-27 cycle-by-cycle to determine $\hat{P}_1$ through $\hat{P}_{\ell-1}$. This solution approach is essentially an extension of Newton's method to the multirate case. Newton's method offers quadratic convergence of the solution as opposed to linear convergence that would be obtained by propagating Eqs. 2.3-26 and 2.3-27 to steady-state; hence, Newton's method is computationally more efficient than direct propagation of the Ricatti equation. Figure C-1 is a flow chart of the present solution method; the notation $(X)_i$ indicates the i^{th} iterative value of variable X.

Note that an initial value, $(\hat{P}_\ell)_0$, is required to start the algorithm. This starting value must yield a stable θ_1^* matrix, otherwise a solution to Eq. C-8 will not exist. A method for generating a stable starting solution for the single rate case is presented in Ref. 12; that method is extended here to the multirate case.

The generation of an initial value of $\hat{P}_\ell$ is accomplished by the following steps:

- The system dynamics are formulated over a complete control cycle.
- An initial value of θ^* is computed using the full cycle plant dynamics and the method of Ref. 12.
- A set of gains, C_k, is generated over the ℓ cycle period using intermediate computations from the second step.
- An initial value of Q^* is computed using the gain set computed in the third step.

R-61248

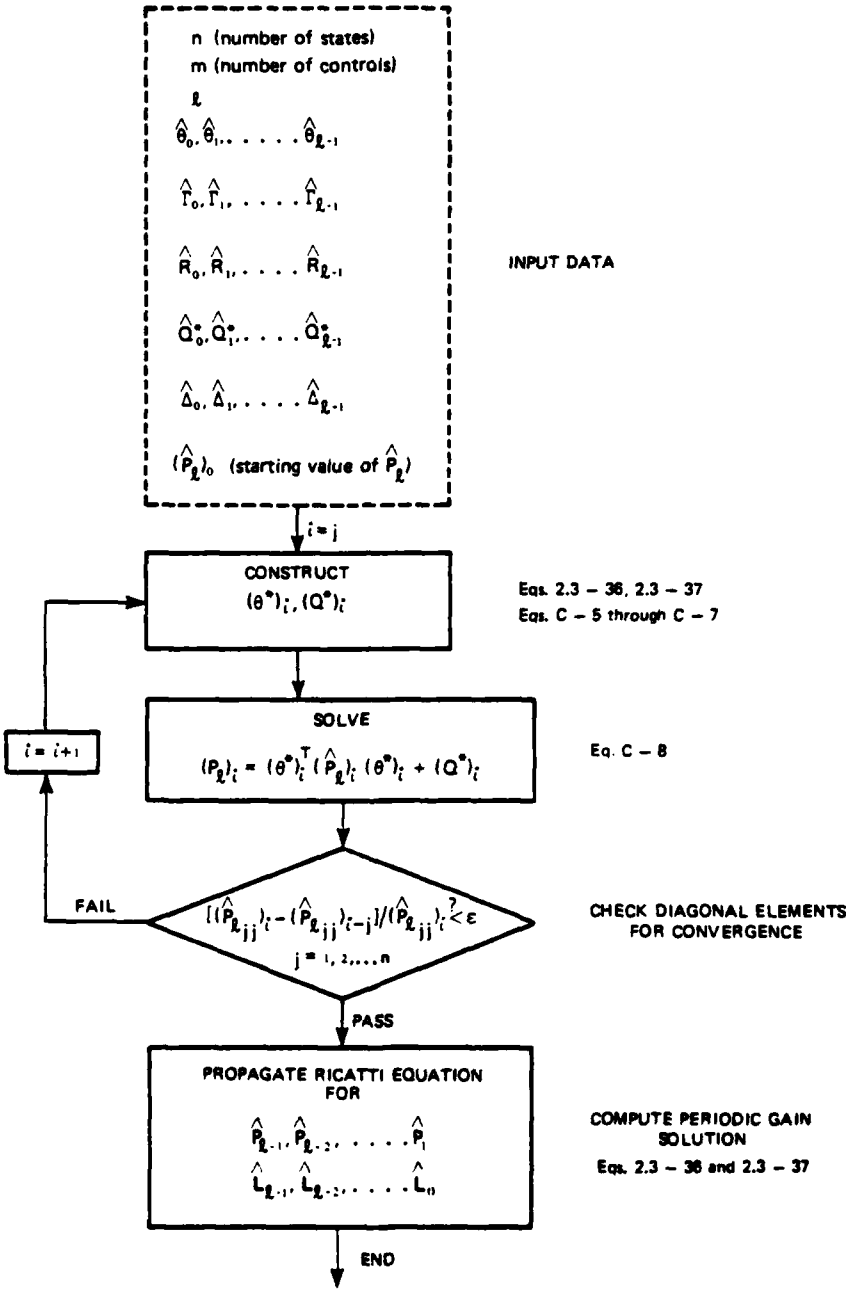

Figure C-1 Newton's Method Algorithm

- Equation C-8 is solved to generate the initial value of $\hat{P}_{\ell}$

The dynamics of the plant over the ℓ cycle period can be described by:

$$\underline{x}_{k+\ell} = \Phi^{\ell}\underline{x}_k + \left[\hat{\Gamma}_{k+\ell-1} \mid \Phi\hat{\Gamma}_{k+\ell-2} \mid \Phi^2\hat{\Gamma}_{k+\ell-3} \mid \cdots \mid \Phi^{\ell-1}\hat{\Gamma}_k\right] \begin{bmatrix} \underline{u}_{k+\ell-1} \\ \underline{u}_{k+\ell-2} \\ \underline{u}_{k+\ell-3} \\ \vdots \\ \underline{u}_k \end{bmatrix} \tag{C-11}$$

or

$$\underline{x}_{k+\ell} = \Phi^{\ell}\underline{x}_k + \hat{B}\underline{u}_k$$

The control weighting matrix for the plant described by Eq. C-11 is:

$$R^* = \begin{bmatrix} \hat{R}_{k+\ell-1} & 0 & 0 & \cdots & 0 \\ 0 & \hat{R}_{k+\ell-2} & 0 & & 0 \\ \vdots & 0 & & & \vdots \\ \vdots & \vdots & & & \vdots \\ & \vdots & & & \vdots \\ 0 & 0 & \cdots & \cdots & \hat{R}_k \end{bmatrix} \tag{C-12}$$

Using the results of Ref. 12 directly on Eqs. C-11 and C-12 one obtains (setting k=0 with no loss of generality):

$$(\theta^*)_0 = (I+SV_{-1})^{-1}\phi^{\ell} \tag{C-13}$$

with

$$V_{-1} = (\phi^{*T})^n \, W_{n-1}^{-1}\phi^{*n} \tag{C-14}$$

$$W_{n-1} = \sum_{j=0}^{n-1} \phi^{*j}S(\phi^{*T})^j \tag{C-15}$$

$$S = \sum_{i=0}^{\ell-1} \phi^{(\ell-1)-i}\hat{\Gamma}_i\hat{R}_i^{-1}\hat{\Gamma}_i^T(\phi^T)^{(\ell-1)-i} \tag{C-16}$$

$$\phi^* = \phi^{\ell} \tag{C-17}$$

The control gain history is derived from

$$\hat{\underline{u}}_o = -R^{*-1}\hat{B}^T V_{-1}\phi^{\ell}\underline{x}_o \tag{C-18}$$

or

$$\begin{bmatrix} \underline{u}_{\ell} \\ \underline{u}_{\ell-1} \\ \vdots \\ \underline{u}_o \end{bmatrix} = \begin{bmatrix} -\hat{R}_{\ell-1}^{-1}\hat{\Gamma}_{\ell-1}^T V_{-1}\phi^{\ell} \\ -\hat{R}_{\ell-2}^{-1}\hat{\Gamma}_{\ell-2}^T\phi^T V_{-1}\phi^{\ell} \\ \vdots \\ -\hat{R}_k^{-1}\hat{\Gamma}_k^T(\phi^T)^{\ell-1}V_{-1}\phi^{\ell} \end{bmatrix} \underline{x}_o \tag{C-19}$$

It is desired to find the $\underline{u}_i$'s in terms of the $\underline{x}_i$'s to determine the gain set (i.e., the C_i's); this can be accomplished by using the following expression of the plant dynamics:

$$\underline{x}_{\ell-j} = \Phi^{\ell-j}\underline{x}_o + \sum_{i=0}^{(\ell-1)-j} \Phi^{(\ell-1)-j-i}\hat{\Gamma}_i\underline{u}_i \qquad \text{(C-20)}$$

Substituting for the $\underline{u}_i$'s using Eq. C-19:

$$\underline{x}_{\ell-j} = \Phi^{-j}(I + \sum_{i=0}^{(\ell-1)-j} \Phi^{(\ell-1)-i}\hat{\Gamma}_i\hat{R}_i^{-1}\hat{\Gamma}_i^T(\Phi^T)^{(\ell-1)-i}V_{-1})\Phi^{\ell}\underline{x}_o \qquad \text{(C-21)}$$

Solving for $\Phi^{\ell}\underline{x}_o$:

$$\Phi^{\ell}\underline{x}_o = (I + \sum_{i=0}^{(\ell-1)-j} \Phi^{(\ell-1)-i}\hat{\Gamma}_i\hat{R}_i^{-1}\hat{\Gamma}_i^T(\Phi^T)^{(\ell-1)-i}V_{-1})^{-1}\Phi^j\underline{x}_{\ell-j} \qquad \text{(C-22)}$$

Substituting Eq. C-22 into Eq. C-19:

$$\underline{u}_{\ell-j} = -\hat{R}_{\ell-j}^{-1}\hat{\Gamma}_{\ell-j}^T(\Phi^T)^{j-1}V_{-1}(I + \sum_{i=0}^{(\ell-1)-j} \Phi^{(\ell-1)-i}\hat{\Gamma}_i^T\hat{R}_i^{-1}\hat{\Gamma}_i(\Phi^T)^{(\ell-1)-i}V_{-1})^{-1}\Phi^j\underline{x}_{\ell-j} \qquad \text{(C-23)}$$

or

$$C_{\ell-j} = -\hat{R}_{\ell-j}^{-1}\hat{\Gamma}_{\ell-j}^T(\Phi^T)^{j-1}V_{-1}(I + \sum_{i=0}^{(\ell-1)-j} \Phi^{(\ell-1)-i}\hat{\Gamma}_i\hat{R}_i^{-i}\hat{\Gamma}_i^T(\Phi^T)^{(\ell-1)-i}V_{-1})^{-1}\Phi^{j-1}\Phi \qquad \text{(C-24)}$$

$$= \hat{L}_{\ell-j}\Phi \; ; \; j = 1, 2, \ldots \ell \qquad \text{(C-25)}$$

Using the initial gain set given by Eq. C-24 and C-25, $(Q^*)_o$ is computed (Eq. C-10). Finally, $(\hat{P}_\ell)_o$ is computed by solving:

$$(\hat{P}_\ell)_o \; (\theta^*)_o^T (\hat{P}_\ell)_o (\theta^*)_o + (Q^*)_o \qquad \text{(C-26)}$$

Again, $(\theta^*)_o$ computed by the present method will be stable and, hence, a solution to Eq. C-26 will exist.

REFERENCES

1. Sandell, N.R., "Optimal Periodic Sampling Policies for Linear Filtering," TASC Internal Memorandum, August 1977.

2. Whitbeck, R.F., and Hofmann, L.G., "Analysis of Digital Flight Control Systems with Flying Qualitities Applications," Vol. 2, Air Force Flight Dynamics Laboratory, Report No. AFFDL-TR-78-115, September 1978.

3. Konar, A.F., and Lee, J.F., "Analysis of Multiloop, Multirate Digital Control Systems," Proceedings of 1976 IEEE Conference on Decision and Control, Clearwater, Florida, December 1976, p. 446.

4. Saxe, R., "DIGIKON: The Direct Digital Control System Analysis Program for Shuttle," Proceedings of 1976 IEEE Conference on Decision and Control, Clearwater, Florida, December 1976, pp. 455-461.

5. Gran, R., Berman, H., and Rossi, M., "Optimal Digital Flight Control for Advanced Fighter Aircraft," Journal of Aircraft, Vol. 14, No. 1, January 1977, pp. 32-37.

6. Glasson, D.P., and Guha, D.K., "Advanced Adaptive Optics Control Techniques," The Analytic Sciences Corporation, Technical Report No. TR-996-1 (Also Air Force Weapons Laboratory Report No. AFWL-TR-78-8), January 1978.

7. Berry, P.W., Broussard, J.R., and Gully, S.W., "Validation of High Angle-of-Attack Analysis Methods," The Analytic Sciences Corporation, Technical Report No. TR-612-3 (Also Office of Naval Research Report No. ONR-CR215-237-3F), February 1979.

8. Broussard, J.R., Berry, P.W., and Gully, S.W., "Stability and Control Analysis of a V/STOL Type B Aircraft," The Analytic Sciences Corporation, Technical Report No. TR-1259-1 (Also Office of Naval Research Report No. ONR-CR213-162-1F), February 1979.

REFERENCES (Continued)

9. Broussard, J.R., Berry, P.W., and Stengel, R.F., "Modern Digital Flight Control System Design for VTOL Aircraft," The Analytic Sciences Corporation, Technical Report No. TR-804-1 (Also National Aeronautics and Space Administration Report No. NASA CR 159019), March 1979.

10. Stengel, R.F., Broussard, J.R., Berry, P.W., and Taylor, J.H., "Modern Methods of Aircraft Stability and Control Analysis," The Analytic Sciences Corporation, Technical Report No. TR-612-2 (Also Office of Naval Research Report No. ONR-CR215-237-2), May 1977.

11. Anon., "Flying Qualities of Piloted Airplanes," Military Specification No. MIL-F-8785B(ASG), 7 August 1969, pp. 47-52.

12. Kleinman, D.L., "Stabilizing a Discrete, Constant, Linear System with Application to Iterative Methods for Solving the Riccati Equation," IEEE Transactions on Automatic Control, Vol. AC-19, No. 3, June 1974, pp. 252-254.

DISTRIBUTION LIST

Office of Naval Research
800 N. Quincy St.
Arlington, VA 22217
S.L. Brodsky, Code 432 — 4

Office of Naval Research
Eastern/Central Regional Office
495 Summer St.
Boston, MA 02210 — 1

Office of Naval Research
Western Regional Office
1030 E. Green St.
Pasadena, CA 91106 — 1

Naval Research Laboratory
Washington, D.C. 20375
Code 2627 — 3

Naval Air Systems Command
Washington, D.C. 20361
D. Kirkpatrick, AIR 320D — 1
R.C. A'Harrah, AIR 53011 — 1

Naval Air Development Center
Warminster, PA 19874
C.J. Mazza, Code 6053 — 1
C.R. Abrams, Code 6072 — 1

Naval Material Command
Washington, D.C. 20360
Code 08T23 — 1

Naval Weapons Center
China Lake, CA 93555
B. Hardy, Code 3914 — 1

Naval Surface Weapons Center
Silver Spring, MD 20910
J. Wingate, Code R44 — 1

David Taylor Naval Ship R&D Center
Bethesda, MD 20084
Technical Library — 1

Naval Post Graduate School
Monterey, CA 93940
Technical Reports Library — 1
L. Schmidt — 1

Defense Technical Information Center
Building 5
Cameron Station
Alexandria, VA 22314 — 12

Air Force Office of Scientific Research
Building 410
Bolling Air Force Base
Washington, D.C. 20332
G.W. McKemie — 1

Air Force Flight Dynamics Laboratory
Wright-Patterson Air Force Base
Dayton, OH 45433
R. Anderson, Control Dyn. Br. — 1
F. George, Control Dyn. Br. — 1
R. Schwanz, AFWAL/FIGC — 3

Air Force Institute of Technology
Wright-Patterson Air Force Base
Dayton, OH 45433
P. Maybeck — 1

Army Armament R&D Command
Building #18
Dover, NJ 07801
B. Schulman, DRDAR-SCF-DD — 1

NASA Langley Research Center
Hampton, VA 23665
Technical Library — 1
D. Downing, MA 494 — 1
J. Chambers, MS 355 — 1
J. Elliot, MS 152A — 1

Naval Air Test Center
Patuxent River, MD 20670
J. McCue, Code TPS 1

University of Michigan
Dept. of Naval Architecture &
Marine Engr.
Ann Arbor, MI 48109
M.G. Parsons 1

Nielsen Engineering &
Research, Inc.
510 Clyde Avenue
Mountain View, CA 94043
J.N. Nielsen 1

The C.S. Draper Laboratory,
Inc.
555 Technology Square
Cambridge, MA 02139
R.V. Ramnath 1

Michigan State University
Mathematics Department
106-A Wells Hall
Michigan 48824
Prof. Bakhtiar Nitkouti 1

NASA Dryden Research Center
P.O. Box 273
Edwards, CA 93523
Technical Library 1
K. Szalai, Code E-EDC 1

National Transportation Satety Board
Bureau of Technology
Laboratory Services Division
800 Independence Ave. SW
Washington, D.C. 20594
R. Von Husen 1

University of Notre Dame
Dept. of Electrical Engineering
Notre Dame, IN 46556
M.K. Sain 1

Flight Research Laboratory
Dept. of Mechnaical & Aerospace Eng.
Princeton University
Princeton, NJ 08544
R.F. Stengel 1


DATE
ILME